Computational fluid dynamics modeling of catalytic wet air oxidation of phenol in a trickle bed reactor

Prepared by

Tladi Joas Makatsa

Submitted in accordance with the requirements for the degree of

MAGISTER TECHNOLOGIAE

In the subject

CHEMICAL ENGINEERING

At the

University of South Africa

Supervisor(s): Prof CM. Masuku

Co-Supervisor(s): Dr. TA. Ntho

: Dr.SJ. Baloyi

June 2020

Abstract

In this study, phenol was oxidized in a trickle bed reactor operated in a continuous mode using aluminum/zirconia pillared (Al/Zr-PILCs) catalyst. The reactor was connected to a gas chromatography and a sample was taken every 1 h to analyze carbon dioxide emitted. A commercial software (Ansys Fluent) was used to simulate experimental results obtained. The powder catalyst (Al/Zr-PILCs) was wash-coated on a surface of cordierite monolith and dried using different drying mediums. After wash-coating the catalyst, different drying methods were used and two samples were dried in an oven at 40 °C and 60 °C while others were dried using thermally assisted microwave and room temperature. X-ray diffraction peak of natural bentonite shifted from 8.25° to lower angle of 7° and basal spacing increased from 12.44 to 15.15 A° confirming that natural clay was successfully pillared. However, montmorillonite peak disappeared after wash-coating the catalyst on the surface of a support due to the amorphous phase of SiO_2 shielding the peak. The morphology of the catalyst was determined using scanning electron microscopy (SEM) and the results clearly showed that the surface of the catalyst was smooth and no cracks were observed when all drying mediums were used due to hygroscopic nature of glycerol. The sample dried using thermally assisted microwave oven was smoother compared to others due to heat that is homogeneously dispersed inside the microwave.

To test catalyst activity and reaction kinetics, phenol was oxidized in a trickle bed reactor operated at 10 bar and temperatures ranging between (120–160 °C) over Al/Zr-pillared clay catalyst using monolith as a support. To understand the kinetics of the process, different variables were studied including reaction temperature and liquid flow rate. It was concluded that an increase in temperature has a positive impact on phenol conversion, whereas an increase in liquid flow rate has a negative effect. A simple power law model was used to model reaction kinetics and the activation energy was found to be 42.289 kJ/mol. To understand the behaviour of the fluid inside the reactor, a computational fluid dynamics (CFD) model was developed from experimental data using an Euler-Euler model. The model indicated that a hot spot was formed near the center of the reactor due to liquid mal-distribution. Moreover, incorporating monolithic structure in a reactor packing material helped to lower pressure drop due to low velocities inside monolith channels. When the reactor was modeled at 160°C and 10 bar phenol was completely oxidized to CO_2.

Keywords: Kinetics Modeling, Computational Fluid Dynamics modeling, Phenol Oxidation, Reaction Mechanism.

Acknowledgements

I’m very grateful to the National Research Foundation (NRF)/Thuthuka, NRF grant No. 113652 and Mineral Science Council of South Africa (Mintek) under CWO of Wastewater Project No. ADR 31904 for financial support. I would also like to give special thanks to my supervisors Prof Masuku, Dr Ntho and Dr Baloyi for their constructive criticism and guidance, without their help I wouldn’t have accomplished what I have. Special thanks goes to Mr. P. Mafulako, Mr. A. Corfield, Ms T. Khumalo, Mr. S Mavuso and Prof. B Patel for assisting me with ball mill, SEM, BET, XRD analysis and administrative work.

Finally, I would like to thank my mom (Maseta Makatsa) and my siblings for their prayers and support. I would also like to thank my wife (Mmabatho Kopung) and son for moral support and financial assistance during difficult times. And lastly I would like to thank God almighty for giving me strength and courage.

Publications and Presentations

Publications

1. **T J Makatsa**, J Baloyi, T Ntho and C M Masuku, Kinetic study of phenol oxidation in a trickle bed reactor over Al/Zr-pillared clay catalyst, *IOP Conf. Ser.:Mater.Sci.Eng 655* (2019). Doi: 10.1088/1757-899X/655/1/012050

2. **Tladi J. Makatsa**, Jeffrey Baloyi, Thabang Ntho and Cornelius M. Masuku, Catalytic wet air oxidation of phenol: Review of the reaction mechanism, kinetics, and CFD modeling, *Critical Reviews in Environmental Science and Technology (2020).* Doi.org/10.1080/10643389.2020.1771886

3. **Tladi J. Makatsa**, Jeffrey Baloyi and Cornelius M. Masuku, Computational fluid dynamics modelling of phenol oxidation in a trickle bed reactor using 3D Eulerian model. **Submitted for publication in Chemical Engineering Science.**

Presentations

1. Title: Kinetic study of phenol oxidation in a trickle bed reactor over Al/Zr-pillared clay catalyst. **Oral presentation**. Authors: **T J Makatsa**, S J Baloyi, T A Ntho and C M Masuku: Conference: Conference of the South African advanced materials initiative (CoSAami) October 23-25, 2019 Vanderbjlipark (South Africa).
2. Title: Wash-coating of cordierite monolith with novel Al/Zr pillared clay catalyst: For wastewater treatment. **Oral presentation**. Authors: **T J Makatsa**, S J Baloyi, T A Ntho and C M Masuku: Conference: Post graduate symposium for civil and chemical engineering department, 7 November 2019, Florida (South Africa).
3. Title: Wash-coating of cordierite monolith with novel Al/Zr pillared clay catalyst: Comparison of drying methods. **Poster presentation**. Authors: S J Baloyi, **T J Makatsa**, M Govender, T A Ntho and C M Masuku: Conference: Conference of the South African advanced materials initiative (CoSAami) October 23-25, 2019 Vanderbjlipark (South Africa).

Contents

Abstract ii
Acknowledgements iv
Publications and Presentations v
Publications v
Presentations v
Chapter 1: Introduction 1
1.1 Background 1
1.2 Research Motivation 3
1.3 Problem statement and purpose of the study 4
1.4 Research aim and objective(s): 5
1.5 Novelty of the study 5
1.6 Research questions 6
1.7 Outline of the dissertation 6
Chapter 2: Literature Review 7
2.1 Homogenous and heterogeneous systems 7
2.2 Reaction mechanism 9
2.2.1. Indirect Mechanism 10
2.2.2 Direct Mechanism 16
2.3. Operating parameter 20
2.3.1. Effect of temperature 20
2.3.2. Effect of initial phenol concentration 22
2.3.3. Effect of pH 23
2.3.4. Effect of liquid and gas hourly space velocity 24
2.4. Kinetic Model 25
2.5 CFD Modelling 30
Chapter 3: Experimental Methods 33
3.1 Materials 33
3.2 Catalyst Preparation 33
3.3 Acid treatment of cordierite monolith 33
3.4 Wash-coating of cordierite monolith with Al/Zr-PILCs 33
3.5 Characterization techniques 34
3.6 CWAO Experiment 34
3.7 Computational fluid dynamics model 35
3.7.1 Governing equations 35
3.7.2 Mesh 36
3.7.3 Boundary conditions 37
Chapter 4: Results and Discussion 38
4.1 Characterization of the catalyst 38
4.2 Catalyst activity test 42
4.3 Influence of operating parameters 43
4.4 Kinetic model 44
4.5 Euler-Euler computational model 47
Chapter 5: Conclusions and Recommendations 53
5.1 Conclusions 53
5.2 Potential for industrialization 53
5.3 Recommendations 54
Reference 54
Appendix A: Experimental Parameters 66

List of figures

Figure 1: Schematic representation of bentonite clay pillaring process adopted from (Baloyi *et al.*, 2018c). 2
Figure 2: Fluid flow regimes inside the TBR (Ahmed ., 2012). 3
Figure 3: Reaction mechanism for CWAO of phenol in a batch reactor using functionalized carbon material as catalyst proposed by (Wang et al. 2014). 11
Figure 4: Schematic diagram of CWAO of phenol reaction mechanism in the presence of Fe/AC catalyst (Quintanilla et al, 2006). 13
Figure 5: Proposed reaction pathway for the CWAO of phenol in the presence of $CuSO_4$ catalyst (Lal & Garg 2014). 15
Figure 6: CWAO of phenol oxidation reaction mechanism (Zapico et al. 2015). 17
Figure 7: Reaction mechanism of phenol oxidation proposed by (Castaldo et al. 2019) 19
Figure 8: 3D reactor geometry and mesh structure of (a) TBR and (b) monolith. 37
Figure 9: XRD patterns of (a) Natural bentonite clay (b) Al/Zr pillared clay catalyst. 38
Figure 10: XRD patterns of (a) Bare monolith, (b) monolith acid treated with oxalic acid and calcined at 500 °C for 2 h, (c) Al/Zr-PILCs monolith dried at 60 °C, (d) Al/Zr-PILCs monolith dried at 40 °C, (e) Al/Zr-PILCs monolith microwave dried, (f) Al/Zr-PILCs monolith dried at room temperature for six weeks. 39
Figure 11: Cross-section SEM images of the bare monolith (a), monolith acid treated with oxalic acid and calcined at 500° C for 2 h (b) zirconium mapping image (c) and wash coated monolith (d). 40
Figure 12: Backscattered electron x-ray mapping images were taken on the surface of the bare monolith (a), monolith acid treated with oxalic acid and calcined at 500° C for 2 h (b), wash coated monolith (c), and zirconium mapping image (d). 40
Figure 13: Secondary electron images were taken on the surface of bare monolith (a), monolith acid treated with oxalic acid and calcined at 500° C for 2 h (b), wash coated and microwave dried (c), wash coated and oven-dried at 40° C (d), wash coated and oven-dried at 60° C (e) and wash coated and dried at room temperature (f). 41
Figure 14: Phenol removal with time in a trickle bed reactor over Al/Zr-PILCs catalyst supported on a monolith (Experimental conditions: 160 °C, 10 bar, 0.012 m/s). 42
Figure 15: Amount of CO_2 released with time during phenol oxidation in CWAO process. 43
Figure 16: Phenol conversion with liquid flow rate and change in reaction temperature. 44
Figure 17: Graph of In(1-Xph) vs τ at 10 bar and temperatures ranging between 120, 140 and 160 °C. 46
Figure 18: Plot of In(k) versus 1/T at a pressure of 10 bar and temperatures of 120, 140, and 160 °C. 46
Figure 19: Contours of phenol mass fraction (a) and CO_2 profile inside the reactor (b). 47
Figure 20: Phenol mass fraction distribution in a radial direction. 48
Figure 21: Mass fraction of phenol inside the reactor bed 49
Figure 22: Temperature profile along the reactor bed at 160 °C. 50
Figure 23: Radial temperature profile inside the reactor at 160 °C. 51
Figure 24: Axial pressure distribution profile inside the reactor. 52
Figure 25: Pump calibration curve 66
Figure 26: Mass flow controller 66
Figure 27: HPLC phenol retention time. 67
Figure 28: Reactor design. 67

List of tables

Table 1: Performance comparison of the results of phenol oxidation with CWAO using various catalysts. 9
Table 2: Kinetic models proposed for heterogeneous CWAO reaction(Guo & Al-Dahhan 2003)..... 28
Table 3: Activation energies and reaction orders found in literature using different reactors. 29
Table 4: Reactor dimensions and operating conditions 37
Table 5: BET results of the catalyst and support. 42

Chapter 1: Introduction

1.1 Background

Industrial processes use a lot of water which must be treated in the effluent plant before discharging it to the municipal wastewater treatment plant (Adekola & Majozi 2017). Industrial wastewater usually contains a high concentration of toxic organic compounds including phenol and its derivatives (Lal and Garg, 2014; Zuo *et al.*, 2017; Baloyi *et al*, 2018a, 2018b). Phenolic wastewaters originate from a number of industrial processes making it a model pollutant for bio-toxic and non-biodegradable organic pollutants. Moreover, phenol is an intermediate product found in the oxidation of aromatic hydrocarbons (Chicinaş, et al 2018). In addition, it is listed as a priority pollutant by the United States Environmental Protection Agency (Lal & Garg 2014). The use of phenol in petroleum, petrochemical, pharmaceutical, paint, pulp and paper, plastic and refinery industries is common (Masuku & Biegler 2019; Baloyi et al. 2018a; Seadira et al. 2018; Villegas et al. 2016; Sun et al, 2015).

There are different wastewater treatment methods available such as, biological (Krastanov *et al*, 2013; Pradeep *et al.*, 2015; Alves *et al.*, 2017; Zhou *et al.*, 2018), adsorption (Frascari et al. 2019; Sun et al. 2019; Luo, et al 2015), electrochemical oxidation (Abbas & Abbas 2019; Liu et al. 2019), incineration (Wang, et al 2019; Ye, et al 2011), reverse osmosis (Al-Obaidi *et al.*, 2017; Al-obaidi *et al.*, 2019a, 2019b) and advanced oxidation processes (Cao et al., 2018; Dewidar *et al.*, 2018; Radwan *et al.*, 2018). Microbial degradation is unsuitable for wastewater that has high concentration of phenol because of its toxicity. Moreover, the process produces a byproduct that poses environmental problems such as activated sludge (Krastanov *et al.*, 2013; Yu et al., 2016; Guerra-que *et al.*, 2019). Incineration is energy-intensive and is only applicable when waste has a chemical oxygen demand (COD) of at least 300 g/L (Cybulski 2007). On the other hand, reverse osmosis produces a concentrated and smaller waste making disposal easy however, the costs of membrane replacement and energy requirement are high (Crini and Lichtfouse., 2019; Pervov and Nguyen., 2019; Tałałaj *et al.*, 2019). The incapability of traditional methods to effectively remove refractory organic wastewater makes it clear that there is an urgent need to develop more efficient and economic processes for treating refractory wastewater before discharging it to water bodies.

Advanced oxidation processes (AOPs) such as catalytic wet air oxidation (CWAO) offer an alternative solution for treating refractory wastewater. CWAO gained a lot of interest over the past two decades because of its ability to oxidize toxic wastewater and complete mineralization of organic pollutants (Fortuny *et al.*, 1995; Maugans and Akgerman., 2003;

Suárez-Ojeda *et al.*, 2007; Monteros *et al.*, 2015; Baloyi *et al.*, 2018b). Moreover, CWAO is a heterogeneous process, so an additional stage of separating the catalyst from the solution is not required in most instances hence making the process more economic (Serra-Pérez et al., 2019). However, the process has some disadvantages like leaching and sintering of active material at high temperature and low pH. Therefore, the use of highly active, stable and inexpensive catalysts will make the technology more feasible.

The use of pillared clays (PILCs) in heterogeneous CWAO is gaining a lot of interest due to low cost and improved surface area of the catalyst. In a normal process, natural bentonite is modified by forming metal oxides pillars which transform the structure to form high surface area micro-porous cross-linked layers. Figure 1 show different stages followed to synthesize Al/Zr-PILCs catalyst. PILCs are known to have high acidity and thermal stability making them preferable for most processes (Mohino, et al 2005). However, PILCs are limited to laboratory applications as there is great difficulty in shaping them from powders to commercial shapes (Baloyi *et al*, 2018a). The use of monolith in heterogeneous catalysis is common because they can be easily scaled-up and the conditions within individual channels remain the same when the catalyst is scaled up (Cybulski., 2007).

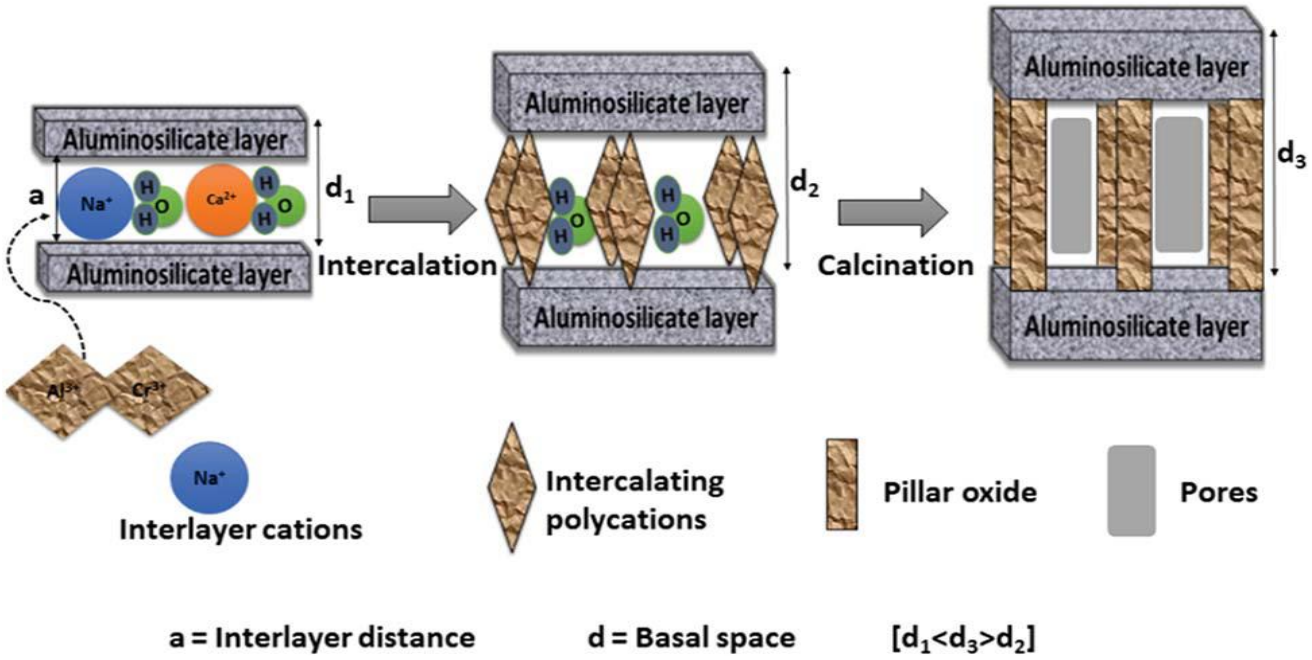

Figure 1: Schematic representation of bentonite clay pillaring process adopted from (Baloyi *et al.*, 2018c).

Furthermore, monolithic catalysts are used in flow reactors mainly because of low-pressure drop, mechanical stability, uniform flow, high external surface area and low axial dispersion (Baloyi., 2019). Trickle bed reactor (TBR) is one of the most used flow reactors in chemical

and petrochemical industry (Moghaddam *et al.*, 2019; Zhang *et al*., 2019). TBR are normally operated in two flow regime namely, low interaction (trickle flow) and high interaction regime (pulse, spray or bubble) as shown in Figure 2. The main challenges associated with the use of this reactor are; liquid mal-distribution resulting in channeling and the formation of hot spots when the reaction is exothermic. The formation of hot spots may result in catalyst deactivation and reactor thermal ran away. In this study, computational fluid dynamics (CFD) is used to model the reaction and to predict the formation of hot spots.

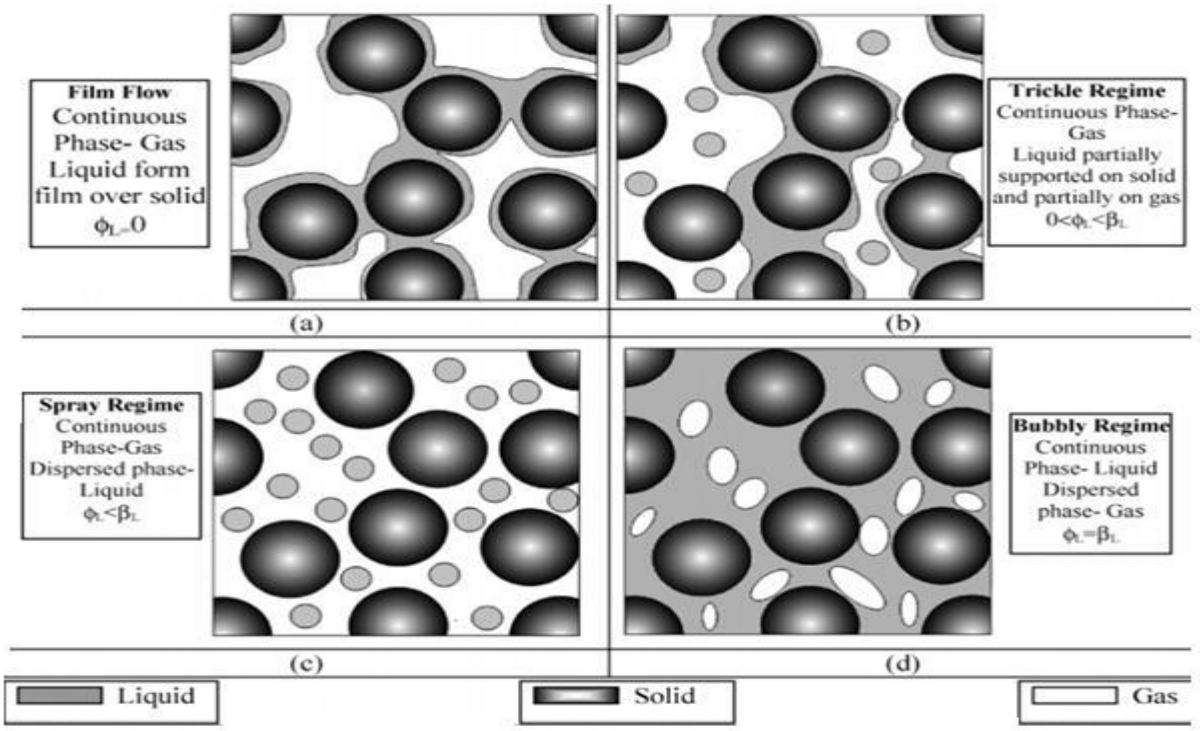

Figure 2: Fluid flow regimes inside the TBR (Ahmed ., 2012).

1.2 Research Motivation

TBR is widely used in many industrial processes and in this reactor both liquid and gas flow co-currently downward. However, there are few challenges associated with this type of reactor such as measuring the interaction between gas, liquid and solid. The reactor flow regime is dependent on superficial mass velocity, fluid properties (density, viscosity, etc.) and design parameters. In most instances, the reactor is operated between low and high interaction regime. Low interaction regime is characterized by low gas-liquid velocities and less gas-liquid interaction while high interaction regime is the opposite. These flow regimes are directly linked to kinetics and hydrodynamics of the reactor. The complex interaction of fluid dynamics and reaction kinetics makes scaling up of laboratory reactors to industrial reactors

very difficult. Moreover, changes in hydrodynamic parameters are significant when laboratory reactors are scaled up to commercial reactors and correlations developed in a laboratory reactor might not work. Ranade et al, (2011) suggested that the scale of the reactor affects the performance of a TBR and they also listed several factors that are directly affected. These authors listed the following factors as the most affected during up-scaling; reactor to particle diameter ratio, reactor volume, bed porosity, wetting, channeling, liquid mal-distribution, dispersion and reactor operating mode (isothermal/adiabatic). Moreover, wall effect is predominant in laboratory TBR whereas flow mal-distribution is common in industrial reactors due to large bed diameter. On the other hand, CFD models should be independent of the scale of the reactor when the design is correct. These models are based on conservation of mass, energy and momentum. In this study, a CFD model was developed to predict phenol degradation in a laboratory reactor and the results will be used to understand the behavior of the process in the industrial scale.

1.3 Problem statement and purpose of the study

The High-Level Panel on Water (HLPW) estimated that 36 % of the world's population resides in water scares areas and half of the world's population will be at risk by 2050 (Zhuwakinyu and the Research Unit of Creamer media., 2018). Over the last ten decades, water usage increased by a factor of six and it is continuing to increase at a constant rate of about 1 % annually due to population growth and economic developments (United Nations World Water Assessment Programme., 2018). By 2017 world population was reported to be 7.7 billion and this number is expected to be between 9.4 and 10.2 billion by 2050 and more than half of forecasted population growth is expected to be in Africa with population of around 1.3 billion followed by Asia with 0.75 billion (United Nations Department of Economic and Social Affairs., 2017). Currently, about 70 % of water worldwide is used for agricultural purposes and 20 % is used for industrial applications and domestic activities account for 10 %. Most of the industrial water is used in the energy sector which accounts for 75 % and the remaining 25 % is used in manufacturing (Zhuwakinyu and the Research Unit of Creamer media., 2018). Industrial wastewater usually contains a high concentration of refractory organic compounds including phenol and its derivatives (Baloyi et al., 2018a,b; Zuo et al., 2017; Lal & Garg., 2016). Phenol is highly soluble in water and industrial wastewater contain phenol in the range of 200-1500 mg/l while Environmental Protection Authority's limit for wastewater discharge is 0.5 mg/L for surface water and 1 mg/L for sewerage water (El-Ashtoukhy et al., 2013).

There are different methods available for the treatment of industrial water such as adsorption, reverse osmosis, biological, incineration and CWAO. The use of these methods is constrained by high capital cost, high maintenance cost, high energy consumption and expensive catalysts. The use of heterogeneous catalysts in CWAO makes the process more attractive because additional cost of separating the catalyst is eliminated. Baloyi (2019) reported that South Africa has bentonite clay reserves that can last for more than 60 years if mined at the current rate of 120 kiloton/annum. The application of pillared clays (PILCs) as a green catalyst in AOPs, has gained a lot of interest because they are cheap, abundant and naturally occurring. However, commercialization of PILCs is challenging because when the conventional method is used production can take days and large volumes of water are used. Another problem associated with the industrialization of PILCs is that the properties of the powder catalyst must be exactly the same as the up-scaled commercially shaped catalyst (pellet or monolith).

In this study naturally occurring South African bentonite clay was used to produce PILCs catalyst and innovative techniques such as ultra-sonication were used to reduce processing time. Furthermore, dry clay was added directly to the pillaring solution to lower water consumption and cordierite monolith was used as catalyst support.

1.4 Research aim and objective(s):

The main aim of this research was to study hydrodynamics and kinetics of a trickle bed monolith reactor and model the behavior of the process.

In order to achieve this aim, the specific objectives of this study are:

1. To synthesis and characterize Al/Zr pillared clay monolith catalyst
2. To investigating the kinetic parameters of the system (phenol) with effects of operating conditions (Temperature and Liquid velocity).
3. To develop a CFD model using ANSYS Fluent software to predict phenol degradation and temperature profile inside the reactor.

1.5 Novelty of the study

There are few studies that focus on preparation and characterization of PILCs catalyst and its use in CWAO of refractory organic pollutants. However, no study in literature so far reported on the use of South African bentonite clay PILC- monolithic catalyst used on CWAO of phenol in a TBR. To the best of our knowledge, this is the first study to simulate CWAO of phenol using a novel Al/Zr-PILC catalyst supported on a cordierite monolith.

1.6 Research questions

This study will attempt to answer the following questions;

I. What is the effect of temperature on phenol conversion?
II. What is the effect of liquid flow rate on phenol conversion?
III. Is there a difference between experimental and CFD results?

1.7 Outline of the dissertation

In **Chapter 1,** a detailed background, problem statement, research motivation, main and specific objectives are covered.

In **Chapter 2**, detailed literature review about reaction mechanism, kinetics, homogeneous and heterogeneous processes and CFD modeling. This chapter was published as; **Tladi J. Makatsa**, Jeffrey Baloyi, Thabang Ntho and Cornelius M. Masuku, Catalytic wet air oxidation of phenol: Review of the reaction mechanism, kinetics and CFD modeling, Critical reviews in environmental science and technology (2020).

In **Chapter 3,** synthesis and characterization of Al/Zr pillared clay catalyst is presented. The results of this chapter were presented in a conference of South African advanced material initiative (CoSAami), 2019; SJ Baloyi, **TJ Makatsa**, M Govender, TA Ntho and CM Masuku, Wash-coating of cordierite monolith with novel Al/Zr pillared clay catalyst: Comparison of drying methods.

In **Chapter 4,** activity test and kinetics study of phenol was performed in a TBR over Al/Fe pillared clay catalyst. This chapter has been published as; **TJ Makatsa**, J Baloyi, T Ntho and CM Masuku, Kinetic study of phenol oxidation in a trickle bed reactor over Al/Zr-pillared clay catalyst, IOP Conf.Ser:Mater.Sci.Eng (2019).

In **Chapter 5** give a summary of conclusions and recommendations for future studies.

Chapter 2: Literature Review

2.1 Homogenous and heterogeneous systems

Numerous researchers have reported salts of Fe, Cu and Mn-based catalysts as commonly used homogenous catalysts in CWAO process, due to remarkable performance for degradation of phenol at lower temperature (120–180 °C) and lower pressure (5–80 bar) (Gao *et al.*, 2018; Trinidad *et al.*, 2019; Guerra-que *et al.*, 2019). Moreover, the process control and reactor design of homogenous catalysts is reported to be less complex as compared to the heterogeneous CWAO process. Arena *et al.*, (2010) found that Fe-, Cu- and Mn-based catalysts were able to remove phenol at oxygen partial pressure of 9 bar, temperature of 150 °C and reaction time of 360 min. Parvas et al., (2014) reported that the $CuO/CeO_2–ZrO_2$ nanocatalysts synthesized via co-precipitation and ultrasound-assisted method was able to achieve complete conversion of phenol with initial phenol concentration of 1000 mg/L at 160 °C and atmospheric oxygen partial pressure after 180 min. Garg and Mishra (2013) reported 90% degradation of phenol over $CuSO_4$ as homogenous catalyst by CWAO process at 120 °C and 5 bar pressure after 4 h reaction time. The homogenous catalysts have proven to be highly active for the phenol degradation and total organic carbon (TOC) removal at lower temperature and lower pressure. However, the homogenous catalyst system is not economically viable due to additional separation steps of dissolved ions after CWAO process which would increase surplus equipment and cost required. Therefore, finding an alternative catalytic system for phenol oxidation which is effective, high energy efficient and cheap with the potential to treat phenol and other highly toxic organic pollutants is important. In this case, the heterogeneous CWAO process has been reported by various researchers as the most promising process for phenol oxidation on large scale applications due to its simplicity in separation and operation.

Recently, numerous heterogeneous catalysts such as noble metals, non-noble metals and metal oxides have been used. The catalytic activities of the various catalysts in the CWAO reaction of phenol are summarized in Table 1. Various researchers have synthesized different heterogeous catalysts with the aim of discovering robust, cheap and efficient solid catalysts, ensuring the total oxidation of highly toxic and recalcitrant in wastewater at mild reaction conditions (Davies et al 2018; Ukonu 2018). For example, Yang *et al.*, 2012 studied the CWAO of phenol at 155 °C and 25 bar pressure using Multi-walled carbon nanotubes (MWCNTs) functionalized by different oxidants (HNO_3/H_2SO_4,H_2O_2,O_3 and air). All

functionalized catalysts showed good catalytic activity, whereas the O_3-treated MWCNTs had the highest activity with 100% phenol and 80% TOC removals after 120 min reaction. Furthermore, the O_3-treated MWCNTs showed high stability in the cyclic reactions. It was suggested that the high amount of carboxylic acid groups and weakly acidic nature of the surface on the functionalized MWCNTs play a significant role for the superior catalytic activity of the MWCNTs. Arena *et al.,* (2012) studied phenol oxidation over MnOx-CeO_2 catalyst and found that the catalyst was highly active at mild temperatures of 100 °C and a total pressure of 10 bar. It was reported that complete phenol removal was achieved within 40 min reaction time, while 80% of TOC conversion was achieved after 60 min. The high catalytic performance of the catalyst was attributed to the rapid adsorption of phenol and its intermediates. The treatment of phenol oxidation was studied by Lai *et al.,* 2019 using Cu_3-Al-500 at 120 °C and 10 bar pressure. The catalyst was found to be stable and complete conversion of phenol and 99% COD was achieved within 120 min. Good catalytic performance was attributed to the redox transitions of Cu^{2+}/Cu^{+} and/or the formation of H_2O_2 and the surface acidity of the catalyst in reaction mixture. Yang *et al.*, 2014 studied the treatment of phenol by CWAO process at 155°C and 25 bar pressure using graphene oxide (GO) and chemically reduced graphene oxides (rGO). The phenol conversion of 100% and mineralization of 84% and 80% was observed with GO and rGO, respectively. High catalytic performance was because of increased surface area and big pore volume of graphene which improves adsorption capacity of the catalyst. de los Monteros *et al.*, 2015 studied CWAO of phenol over Ru and Pt supported on TiO_2–x wt% CeO_2 at 155°C and 20 bar pressure. The (Ru,Pt)-TiO_2–CeO_2 catalysts showed high activity towards oxidation of phenol by achieving 100% phenol conversion and 88% TOC removal. Baloyi *et al*, 2018 reported the complete removal of phenol and 88% TOC removal after 120 min at 100 °C and 10 bar over low-cost Al/Zr-PILCs catalyst. The catalyst was very stable and a negligible amount of Zr^{4+} was found in the leachate after six runs.

Table 1: Performance comparison of the results of phenol oxidation with CWAO using various catalysts.

Catalyst	Reactor	Conditions	Effect	Ref.
MWCNTs	Batch	155 °C, 25 bar, 1000 mg/L, 120 min	100% phenol removal, 75% TOC removal	(Yang et al., 2012)
MnO_x-CeO_2	Autoclave	140 °C, 20 bar, 1000 mg/L, 60 min	100% phenol removal, 98% TOC removal	(Arena *et al.*, 2012)
Cu_3-Al-500	Autoclave	120 °C, 10 bar, 2000 mg/L, 120 min	100% phenol removal, 99% COD removal	(Lai et al., 2019)
GO	Batch	155 °C, 25 bar, 1000 mg/L, 120 min	100% phenol removal, 84% TOC removal	(Yang et al., 2014)
rGO	Batch	160 °C, 7 bar, 1000 mg/L, 120 min	100% phenol removal, 80% TOC removal	(Yang et al., 2014)
(Ru,Pt)-TiO_2–CeO_2	Batch	160 °C, 20 bar, 2098 mg/L, 180 min	100% phenol removal, 88% TOC removal	(de los Monteros et al., 2015)
Al/Zr-PILCs	Autoclave	100 °C, 10 bar, 1000 mg/L, 120 min	100% phenol removal, 88% TOC removal	(Baloyi *et al.*, 2018)

2.2 Reaction mechanism

The reaction mechanism of phenol oxidation is a complex process resulting in the formation of aromatics, lightweight carboxylic acids and inorganic compounds (CO_2 and H_2O). The reaction mechanism requires an understanding of the reactions that take place on the surface of the catalyst together with intermediates and final oxidation products (Braga et al., 2018). In most instances, phenol oxidation takes the following route; oxidation, decarboxylation, dehydration or combination of all steps (Eftaxias, 2002). According to Eftaxias (2002), the relevant phenol oxidation reactions at the catalyst surface causing the oxidation of phenol can be expressed as follows:

$$RH - OH + cat \longrightarrow R \bullet H = O + \bullet H - cat \quad (1)$$

$$R \bullet H = O + O_2 \longrightarrow RHO - OO \bullet \quad (2)$$

$$RHO - OO \bullet + RH - OH \longrightarrow ROH - OOH + R \bullet H = O \quad (3)$$

where RH − OH represents phenol, R • H = O is phenoxy radical while RHO − OO• corresponds to peroxy radical.

Several studies have been conducted by different researchers with the aim of determining intermediate species formed on the surface of the catalyst. The findings are still controversial because some scholars reported that phenol can be directly oxidized to CO_2 and H_2O (Figure 6 & Figure 7) without the formation of intermediates while others claim the formation of polymerization product (Figure 5) and acetic acid via an indirect mechanism. In some instances, acetic acid can be fully oxidized to CO_2 and H_2O while in some cases it is resistant to the oxidation process.

2.2.1. Indirect Mechanism

Wang et al., (2014) proposed a different mechanism from the ones in literature, they used functionalized carbon materials as catalysts (multi-walled carbon nanotubes, nanofibers, and graphite) to investigate phenol oxidation. Phenol was oxidized in a 1 L autoclave reactor equipped with a stirrer, heating device and cooling coil. The reactor temperature and pressure were kept constant at 160 °C and 25 bar. To identify intermediates they used HPLC with 60 % methanol in water plus 0.1 % acetic acid as mobile phase and ODS-3 column. The removal of phenol over this catalyst reached almost 100 % after 120 min, suggesting that these catalysts are very active. The results obtained can be attributed to carboxylic acids found on the surface of functionalized carbon material improving their activity. In their study, catechol was not detected like in most papers in open literature and they suggested that it might be because of different catalysts used. Maleic, fumaric and very low concentrations of cis butenedioic anhydride were also detected. To further understand the reaction path; pure standards of maleic, malonic, acetic, oxalic and formic acid were also oxidized. In CWAO of maleic acid, the following intermediates were found; malonic acid, oxalic acid, acetic acid, and formic acid. Acetic acid was not detected in the first 30 min of the experiment showing that it is not directly produced from the oxidation of maleic acid instead it might be produced from malonic and oxalic acid. In the oxidation of malonic acid, a sharp decrease in concentration was observed while both acetic and formic acids were shortly detected in the solution suggesting that these two are direct products of malonic acid oxidation. Two peaks were detected by HPLC when acetic acid was oxidized, one was assigned to acetic acid and the other one was unknown. An assumption was made that this unknown peak belongs to dioxirane but it was never confirmed since dioxirane of high purity was not available. Oxidation of formic acid follows the same route as the one reported by Santos et al., 2002.

Santos et al., (2002) proposed a mechanism for formic acid oxidation and suggested that it follows a termination path in the free radical mechanism whereby hydroxyl radical attacks it to remove hydrogen bonded to carbon and the free radical •COOH to form oxalic acid. Moreover, they found that when conditions are suitable, formic acid and oxalic acid mutually interconvert. After careful considerations the authors proposed a reaction path in Figure 3.

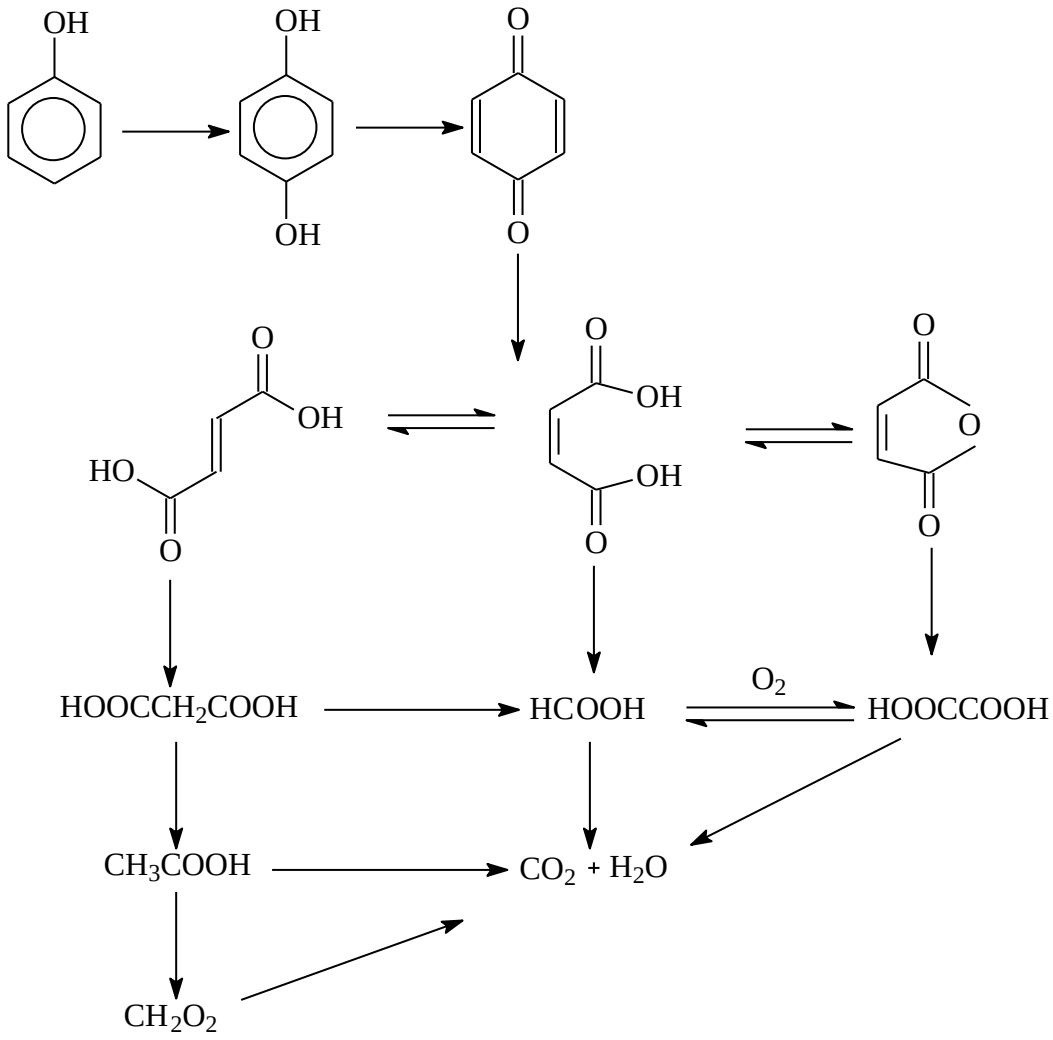

Figure 3: Reaction mechanism for CWAO of phenol in a batch reactor using functionalized carbon material as catalyst proposed by (Wang et al. 2014).

Quintanilla et al., (2006) proposed a reaction pathway shown in Figure 4 for phenol oxidation over Fe supported on activated carbon (AC) catalyst. The proposed study was carried out in a trickle bed reactor with an inside diameter of 8.5 and 305 mm length and the reactor was operated between (100 °C, 127 °C and 8 bar), pressure and flow rates were kept constant by mass flow controller and back pressure valve. Phenol and other intermediates were measured by HPLC using Nucleosil C_{18} column (15 cm, 4.6 mm, 5 µm) with a mobile phase of 4 mM

sulphuric acid mixed with acetonitrile (9:1, v/v). During CWAO of phenol calculated values of total organic carbon (TOC) were higher than the measured ones at low reaction times, indicating that there are some unidentified intermediates. These unidentified intermediates were assigned to condensation products belonging to aromatics or quinone-like since a strong brownish color was observed. At high reaction times, these compounds were not present since calculated TOC results were in agreement with measured results and this was confirmed by a colorless solution.

The formation of p-hydroxybenzoic acid follows two routes: it can be formed when phenol interacts with oxygen groups found on the surface of activated carbon or from the oxidation of chemically adsorbed species on the surface of AC previously formed by oxidative coupling reaction of phenol and aromatics. During oxidation of intermediates, 90 % of hydroquinone was converted to p-benzoquinone. When p-benzoquinone was oxidized 100 % conversion was achieved with maleic, malonic, acetic and formic acid identified as intermediates. However, a small difference was observed between TOC and p-benzoquinone conversion values in the reactor exit. Thus, suggesting that most of p-benzoquinone was converted to CO_2 and H_2O via oxalic acid. Oxidation of p-hydroxybenzoic acid produced maleic, acetic and formic acid. Unidentified species were neglected due to close values of measured and calculated TOC. Maleic acid was the main product of oxidation. At high reaction time, 100 % of oxalic acid was converted to CO_2 and H_2O. In addition, oxidation of maleic acid produced fumaric, acetic and formic acid whereas formic acid concentrations were higher than acetic acid at TOC values ranging between 20 and 40 %. The measured and calculated TOC values were in agreement indicating complete oxidation of maleic acid. Formic acid was completely mineralized when it was oxidized at 127 °C and 8 bar whereas no conversion was observed when acetic acid was oxidized. Furthermore, malonic acid was oxidized to acetic acid and CO_2. However, traces of formic acid were detected but measured and calculated TOC values indicated that all intermediates were identified.

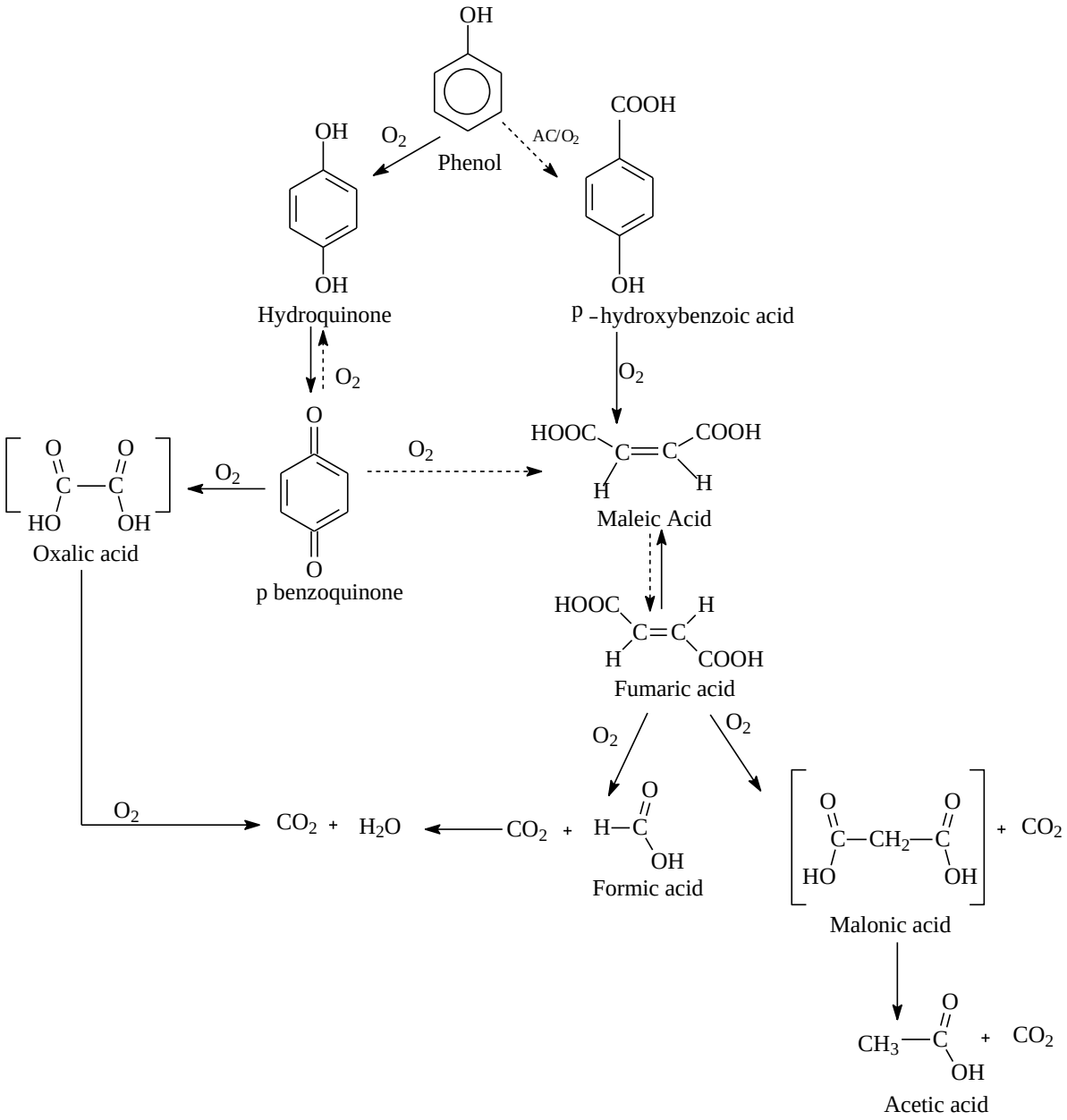

Figure 4: Schematic diagram of CWAO of phenol reaction mechanism in the presence of Fe/AC catalyst (Quintanilla et al, 2006).

Lal and Garg (2014) investigated phenol oxidation under mild operating conditions (120 °C and 5 bar) using a homogeneous copper catalyst in a 0.7 L high-pressure stainless steel batch reactor equipped with a stirring rod. The reactor was equipped with a heating jacket and the temperature was regulated using a proportional integral derivative (PID) controller. Similarly, they used HPLC to measure intermediates and Synergi C_{18} column (25 cm, 4.6 mm, 4 µm). Phosphate buffer was mixed with acetonitrile (9:1, v/v) and used as a mobile phase. Phenol was completely oxidized within 30 min and parallel reaction pathway was confirmed by the appearance of hydroquinone and catechol. Samples collected between 15 and 30 min showed the presence of p-benzoquinone due to breaking down of hydroquinone. However, o-

benzoquinone was not detected when catechol was oxidized due to the unstable nature of this compound caused by two adjacent C=O groups. All organic acids (oxalic, formic, malonic, maleic and fumaric) were detected within 15 minutes except acetic acid which appeared after 30 min. Acetic acid is formed during decarboxylation of malonic acid and oxalic acid might break down to formic acid during this process. Moreover, traces of maleic and fumaric acids were also detected and a significant concentration of oxalic acid was found after 3 h. In addition, formic acid was decarboxylated by hydroxyl radicals to form CO_2 and H_2O and the authors proposed a mechanism in Figure 5. The reaction of hydroxyl radical can happen in three ways: by hydroxyl addition, hydrogen abstraction or electron transfer. In the presence of transition metals, CWAO follows auto-oxidation mechanism in this manner:

$$C_6H_5OH \xrightarrow{Cu^{2+}} C_6H_5OH\bullet + H\bullet \quad (4)$$

$$C_6H_5OH\bullet + O_2 \longrightarrow C_6H_5OOO\bullet \quad (5)$$

$$C_6H_5OOO\bullet + H_2O \longrightarrow C_6H_5OOOH + HO\bullet \quad (6)$$

$$C_6H_5OOOH \longrightarrow C_6H_5O\bullet + HO_2\bullet \quad (7)$$

$$C_6H_5O\bullet + C_6H_5O\bullet \longrightarrow C_6H_5OOC_6H_5 \quad (8)$$

Hydroxyl radicals are known to be neutral electrons and they attack at the high electron density area of the molecule. Phenolic compounds have high electron density available at ortho and para positions because of the resonance effect. Due to this effect; hydroxyl radical attacks these positions to remove hydrogen or add oxygen leading to the formation of catechol or hydroquinone. The formation of p-benzoquinone is due to the formation of stable free radical formed when hydroquinone is attacked by the free radical. Benzoquinone has six carbon chains and two have low electron density caused by oxygen electronegativity. The electron density of the other four carbons can be increased by the presence of oxygen by resonance, causing ring opening when $HO^{\bullet}$ attacks these carbons. Some polymers were also identified by Fourier Transmission Infrared (FTIR) microscopy showing the presence of aromatics, olefinic and alcohols.

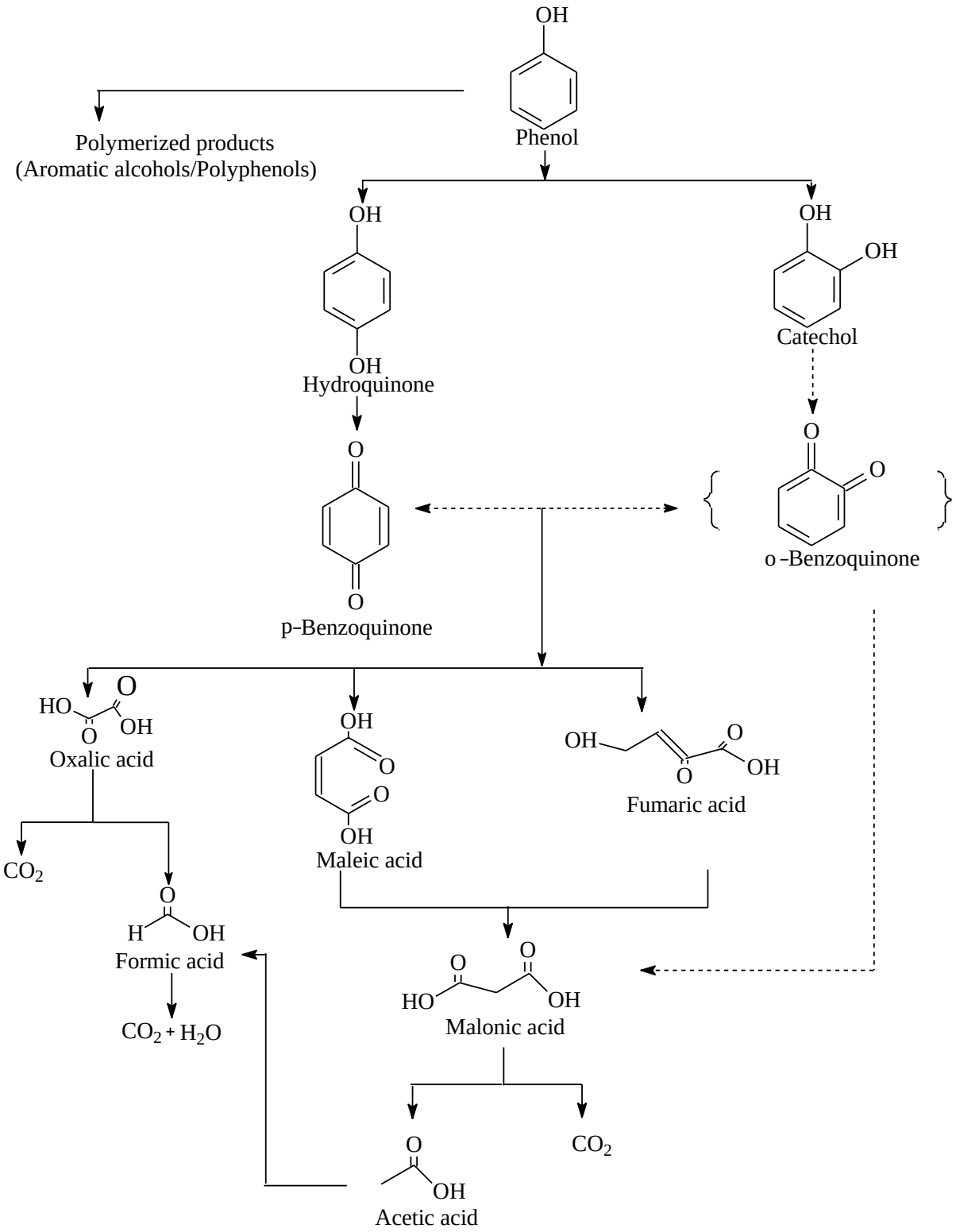

Figure 5: Proposed reaction pathway for the CWAO of phenol in the presence of $CuSO_4$ catalyst (Lal & Garg 2014).

Most of the studies that suggest the formation of polymers as intermediates were performed in a batch reactor at mild operating conditions in the presence of Cu^{2+} catalyst. These polymers are formed due to a high ratio of liquid volume to catalyst in the reactor. When the catalysts

was characterized, the results indicated that polymerization products were present on the surface of the catalyst. These polymerization products reduce the activity and reusability of the catalyst by blocking access to active sites. However, when functionalized carbon materials were used as catalysts at high pressure, polymerization products were not detected and phenol was completely removed. Therefore, the use of a batch reactor in phenol oxidation is not practical due to the high pressure required to avoid the formation of polymers and high costs of catalyst regeneration. On the other hand, when TBR was used, polymerization products were not formed and phenol was completely oxidized. However, when Cu^{2+} catalyst was used, analysis results indicated that Cu^{2+} ions were present in the solution suggesting leaching of the catalyst. Several studies reported that pillared clay (PILC) catalysts are stable and leaching of active sites is insignificant (Guo and Al-Dahhan, 2003; Baloyi et al., 2018a; Moma et al., 2018). Therefore, TBR should be used in the wastewater treatment of phenolic compounds. In order to minimize leaching of active sites, it is advisable to use PILC catalyst in CWAO of phenolic compounds.

2.2.2 Direct Mechanism

Using homogeneous copper catalyst in a 1 L stainless steel batch reactor equipped with three blades of 20 mm propeller, Zapico et al., 2015 proposed a reaction pathway in Figure 6 after oxidizing phenol using the following operating conditions, temperatures (100 – 140 °C) and oxygen partial pressures of (5 – 12.5 bar). The reaction temperature was regulated using a temperature-controlled oven. Their main aim was to determine the influence of operating conditions (temperature, pH, and concentration) on phenol oxidation in acidic conditions. When phenol was oxidized it was reported that a black solid (polymer) was formed when the reaction was prolonged and this solid was insoluble in both polar and non-polar organic solvent. This type of intermediate was also reported by (Levec and Pintar, 1995), and after further testing, they concluded that this intermediate was a polymer. To confirm their results, the authors used GC/MSD and proposed a mechanism that explained the formation of this compound. The authors suggested that polymers are formed by stepwise addition of glyoxal to phenol. In addition, at low pH value of 2 , phenol conversion with time was found to be very low due to the formation of maleic acid and this was explained by the fact that reaction rate is proportional to pH. At low pH, phenol is not oxidized because phenoxyl radicals produced are immediately protonated, avoiding the formation of intermediates. After analyzing the final product, the following intermediates were identified by HPLC using 5% acetonitrile in water as a mobile phase and Agilent Zorbax SB-Aq column (15 cm, 4.6 mm, 5

μm); hydroquinone, p-benzoquinone, catechol, maleic and oxalic acid. Hydroquinone, p-benzoquinone and catechol were completely removed at pH 4 after 5 hours; at lower pH values, high reaction time was required. When COD analysis was performed, it was discovered that oxidation takes place via two paths, direct oxidation of phenol to CO_2 and H_2O and indirect mechanism which involves the formation of intermediates.

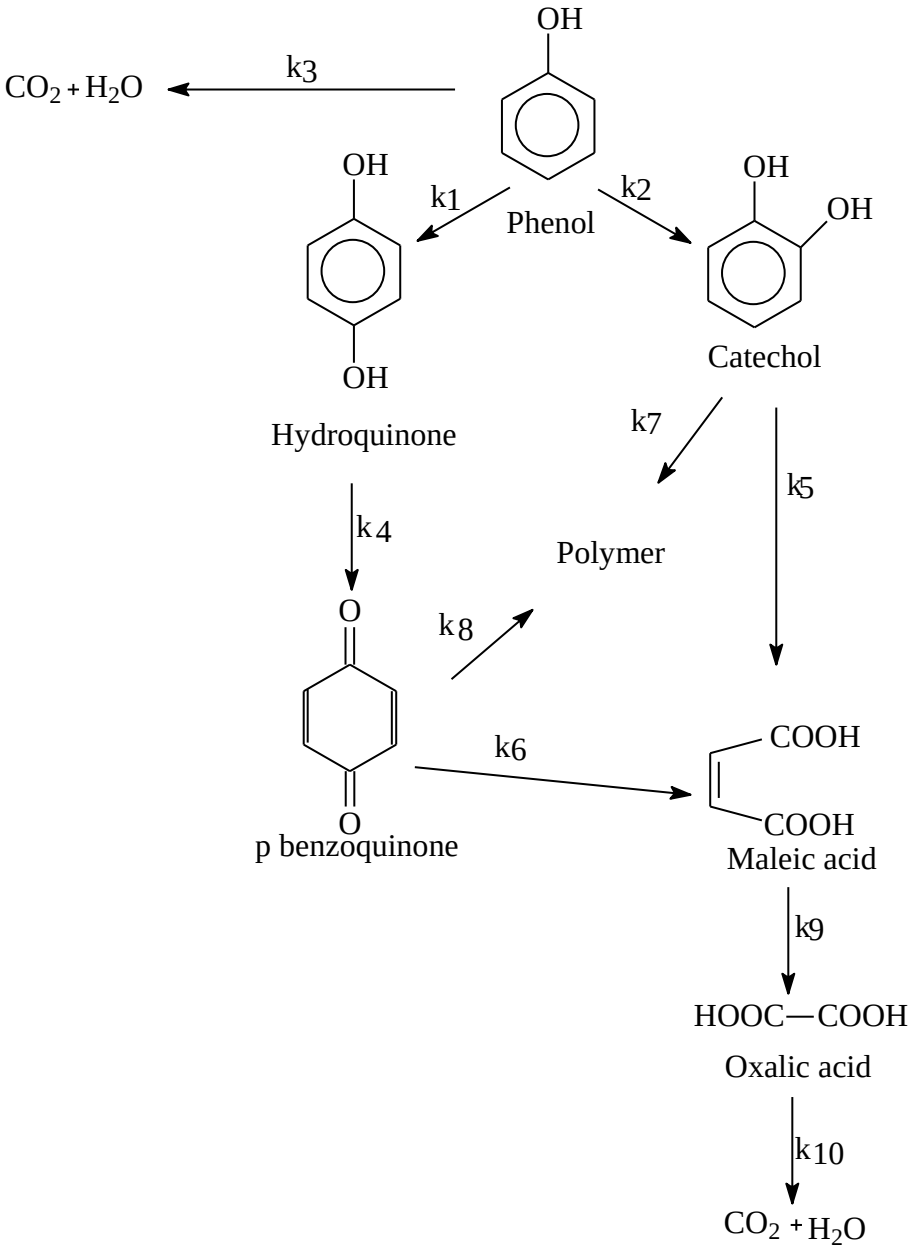

Figure 6: CWAO of phenol oxidation reaction mechanism (Zapico et al. 2015).

Castaldo *et al.*, (2019) investigated phenol oxidation in a glass semi-batch reactor operated at 95 ℃ and 0.3 MPa over a nanocomposite catalyst of $PtRu/MoS_2$ embedded in a hyper-crosslinked resin. The reactor was equipped with a magnetic stirrer and the temperature was

controlled using a heating jacket. In contrast to (Lal and Garg, 2014, Quintanilla et al., 2006), these authors used UV-vis spectra and gas chromatography coupled with a mass spectrometer (GC-MS) to measure phenol conversion. Moreover, carbon dioxide evolution was measured using Siemens Utramar 22 analyzer. To test catalyst activity; two experiments were conducted at 1000 and 4000 mg/L of phenol concentration while keeping operating conditions the same in all experiments. When the experiment was conducted at high concentrations (4000 mg/L) both acetic acid and hydroquinone were detected by UV-vis at low and high wavelengths after 240 min and 99.9 % of phenol was removed. Further tests were performed using GC analyzer and after 300 min, phenol content was 30.1 % and a high concentration of acetic acid (96.61 %) was detected whereas insignificant amounts of hydroquinone (2.98 %) and p-benzoquinone (0.41 %) were detected. These authors proposed a reaction mechanism in Figure 7 and suggested that hydroquinone was the primary intermediate and it oxidizes fast to form p-benzoquinone. Moreover, this intermediate (p-benzoquinone) oxidizes to form CO_2 and carboxylic acids. When low concentration (1000 mg/L) was used, UV-vis spectra indicated the presence of low molecular weight organic acid (acetic) after 30 min and these results were confirmed by GC-MS. Furthermore, 99.9 and 97.1 % of phenol and TOC were removed.

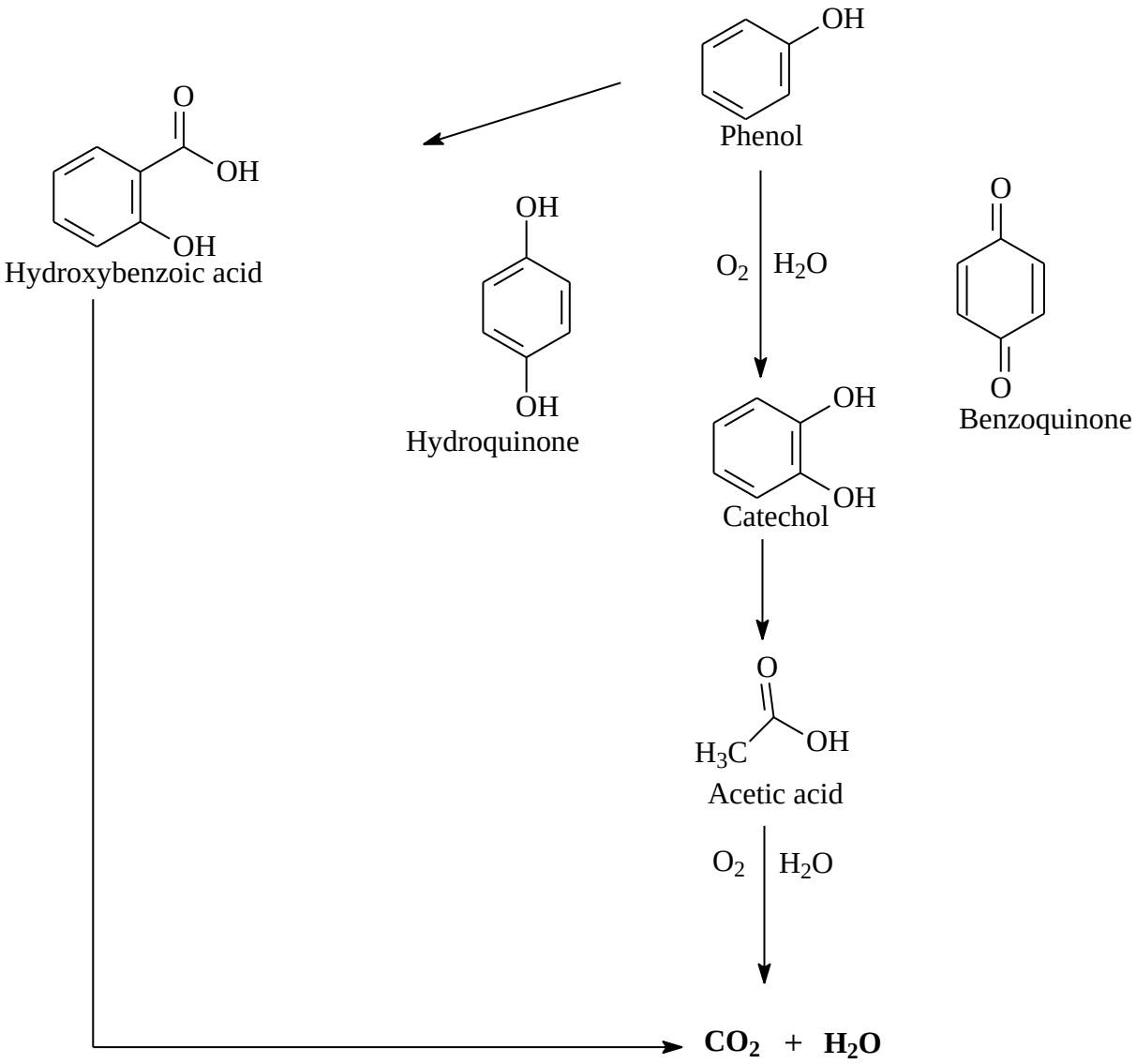

Figure 7: **Reaction mechanism of phenol oxidation proposed by** (Castaldo et al. 2019)

It is interesting to note that Castaldo *et al.*, 2019 managed to oxidize phenol directly to CO_2 and H_2O at mild operating conditions in a batch reactor and no polymers were formed. The catalyst used in their study might be too expensive when the process is scaled up. Similar results were also reported by Zapico et al., 2015 in their study. However, the authors reported the formation of polymerization products. It is therefore, advisable to avoid the use of a batch reactor in a homogeneous process because of the added costs of separating a catalyst at the end of the process. The future research should focus on the development of inexpensive catalysts that are highly selective to CO_2 and H_2O for heterogeneous processes.

2.3. Operating parameter

2.3.1. Effect of temperature

It is generally accepted that an increase in temperature will result in high phenol conversion due to the fact that the reaction rate constant is a function of temperature and activation energy, according to the Arrhenius equation:

$$k = A\exp\left(\frac{-E_a}{RT}\right) \quad (9)$$

Where k is the reaction rate constant, A is a pre-exponential factor, E_a is activation energy, R is the gas constant and T is the temperature.

The increase in temperature also results in the formation of oxygen free radicals which can react with oxygen and water to form peroxide (H_2O_2) and ozone (O_3) radicals. These radicals can participate in phenol oxidation, thus increasing the efficiency of the process (Mohammed, et al, 2016a). The study by Eftaxias et al., 2005 proved that the performance of unsupported commercial activated carbon as a catalyst is highly dependent on temperature. They investigated phenol oxidation using activated carbon as a catalyst in a trickle bed reactor operated between 120 °C - 160 °C. Phenol and COD conversion improved when temperature and space-time were increased resulting in conversions higher than 99 % for phenol, 85 % COD at 160 °C and space-time greater than 0.4 h. Similarly, Mohammed (2014) studied the effect of temperature on phenol oxidation in a trickle bed reactor operated between (120 °C - 160 °C) using activated carbon as a catalyst. After 1 h they reached 100 % conversion at 160 °C while at low temperatures (120 and 140 °C) low conversions were reported (88.6 and 92.7 %). Yang et al., 2014 also used carbon-based catalysts (graphene oxide and reduced graphene) in a batch reactor. The reactor temperature was kept constant at 155 °C and graphene oxide (GO) was found to be the most active catalyst achieving 100 % phenol conversion in 40 min while 120 min was required to remove all phenol when reduced graphene oxide (rGO) was used. Furthermore, over 80 % of TOC was converted after 120 min in both cases. Wu et al, 2005 used copper supported on activated carbon as a catalyst in a batch reactor with a temperature range of (140 °C - 160 °C) and a similar trend was also reported.

Ahmed, 2012 investigated phenol oxidation using 0.5 % Pt supported on γ-Al_2O_3. Phenol was oxidized in a trickle bed reactor operated between the temperatures of 85 °C and 140 °C. They reported phenol conversions of 88.59 %, 75.6 %, 65 %, and 43.86 % at 140 °C, 120 °C, 100 °C and 85 °C, respectively. The formation of intermediates also increased with an

increase in temperature. Mohammed et al., 2016 developed a kinetic model for phenol oxidation in a trickle bed reactor using 0.48 % Pt/ γ-Al_2O_3 spheres as a catalyst and the reactor was operated between (120 °C - 160 °C). In their model kinetics parameters were estimated based on experimental data and from the data obtained they up-scaled the reactor to predict the behavior of phenol oxidation in industrial reactors. At a temperature of 120 °C phenol conversion was 87.954 % and when the temperature was increased to 140 °C and 160 °C phenol conversion increased significantly to 90.878 % and 93.13 %. On the other hand, several authors used less expensive catalysts like MnO_2/CeO_2, Al/Zr pillared clay (PILC), Al/Cr pillared clay, Al/Fe pillared clay, and Al-Fe pillared clay (Hamoudi et al, 1998; Guo and Al-Dahhan, 2003; Mohammed and Abdullah, 2008; Baloyi et al, 2018a; Moma et al, 2018). Baloyi et al, 2018a studied phenol oxidation in a batch reactor operated at 100 °C, over single metal oxide pillared clay (Al-PILC & Zr-PILC)) and mixed metal oxides (Al/Zr-PILC) pillared clay catalyst. After a reaction time of 180 min, 100 % conversion was attained when both single and mixed metal oxide catalysts were used in separate experiments. However, high TOC removal was achieved when the mixed metal oxide catalyst was used (88 %) compared to single metal oxide (61 %) after 180 min. Similar results were also obtained by Baloyi et al, 2018a . Phenol was oxidized in a batch reactor operated at 100 °C using single metal oxide pillared clay (Al-PILC & Cr-PILC)) and mixed metal oxides (Al/Cr-PILC) pillared clay catalyst. After 120 min 100 % phenol was removed when Al/Cr-PILC (1:1 molar ratio) was used and approximately (ca.) 84% of TOC was converted after 180 min whereas when single metal oxides were used TOC conversion decreased from 84 to 36 %. In their study Guo and Al-Dahhan, 2003 studied wet air oxidation of phenol over Al-Fe pillared clay catalyst extrudes. Phenol oxidation was investigated between 90 °C and 150 °C in a basket stirred tank reactor. According to their findings, phenol and its intermediates are highly influenced by temperature increase. Furthermore, it was concluded that a 20 °C increase in temperature can result in double phenol conversion in 1 h. In addition, they managed to remove 0.5 g/L of phenol completely when the reactor was operated at 90 °C for 300 min, whereas at 130 °C phenol was completely removed within 100 min. Phenol conversion was faster compared to intermediates degradation due to the fact that short-chained carboxylic acids are more stable and oxidation rate increase with a molecular weight of the acid (Klinghoffer et al., 1998). Hamoudi et al., (1998) investigated phenol oxidation in a batch reactor under mild conditions (80 °C – 130 °C) using MnO_2/CeO_2 catalyst. They reported 100 % phenol removal at 130 °C after 30 min, while TOC conversion was more than 98 %. An

increase in temperature was less pronounced for intermediates compared to phenol removal indicating the formation of carboxylic acids.

In summary, the studies that were conducted using carbon-based catalysts indicated that at high-temperature phenol was completely removed in a short period. This is because phenol is reduced in two ways, adsorption and catalytic activity. The same results are also evident when PGMs and PILC catalysts are used. However, PGMs are expensive and the reaction temperature required to completely remove the pollutant is high irrespective of the catalyst used. Furthermore, many studies involving the use of PILC catalysts are conducted in a batch reactor. Therefore, more studies should be conducted to develop catalysts that are cheap and highly reactive (PILC) to reduce reaction temperature and space-time using a different reactor configuration (TBR) instead of batch.

2.3.2. Effect of initial phenol concentration

The study of the effect of initial phenol concentration is significant both from a mechanistic and application point of view to investigate the dependence of phenol reaction rate kinetics on the substrate concentration. Mohammed et al., (2016) investigated phenol oxidation in a trickle bed reactor using 0.48 % Pt/ γ-Al_2O_3 catalyst while varying initial phenol concentration from, 0.001, 0.003 and 0.005 g/L. When phenol concentration was increased from (0.001-0.005 g/L), conversion increased from 80.35 to 94.75 % due to increased phenol molecules on the active sites of the catalyst. Similarly, Abid et al., 2014 investigated the effect of initial phenol concentration in a trickle bed reactor over 0.5 % Pt/ γ-Al_2O_3 catalyst while varying phenol concentration between, 0.9, 2.5 and 5 g/L. The authors reported that an increase in phenol concentration has a negative impact on phenol conversion, contradicting the results reported by Mohammed et al., 2016 . Moreover, the conversion of phenol at 0.9 g/L was 67.47 % and when the concentration was increased to 5 g/L the conversion decreased to 59.44 % indicating 8 % reduction. Resini et al., (2008) also investigated the effect of phenol concentration between (0.035-0.118 g/L) over lanthanum strontium manganite catalyst in a batch reactor. According to their observations, phenol conversion decreased with an increase in concentration and they attributed this occurrence to transport limitations of phenol on the surface of a catalyst. Similar results were also reported by Lal and Garg, (2014), the researchers investigated the effect of initial phenol concentration between (1-10 g/L) over the homogeneous copper salt catalyst in a batch reactor. A significant amount of phenol was removed after 3 h with an increase from approximately 60 to 96 %.

Moreover, phenol conversion increased with a decrease in concentration and similar trends were also observed for TOC.

It is generally reported that the phenol oxidation rate increases with an increase in concentration. However, this concept is true to a certain extend because a further increase in concentration beyond a saturation point usually results in a decrease in phenol conversion. This phenomenon is demonstrated in several studies conducted by different scholars to determine the effect of phenol concentration. Their findings are still controversial because some researchers claim that an increase in phenol concentration increases conversion while others report the opposite. These controversial findings necessitate the need to investigate the claim further to close the gap.

2.3.3. Effect of pH

At low pH values the following reaction takes place (Zapico et al. 2015):

$$PhO\bullet + H^{+} \longleftrightarrow PhOH\bullet^{+} \quad (10)$$

Zapico et al., 2015 investigated the effect of pH in a batch reactor operated between pH values of (2- 4) using a homogeneous copper catalyst. According to their findings, phenol conversion increased with an increase in pH. The induction period was also observed at pH 3 and 4 due to the initialization step of radical reactions and this phenomenon decreased with increase in pH. This suggests that phenol is not oxidized at low pH values because initialization reaction produces phenoxyl radicals that are immediately protonated avoiding the formation of intermediates. The reaction rate is heavily dependent on pH, thus an increase in pH affects the reaction rate positively. Abid et al., (2016) investigated the effect of pH in a trickle bed reactor operated between pH values of (3- 10) using activated carbon (AC) catalyst. The highest phenol conversion was achieved at pH 5 whereas when pH was increased to 10, lowest conversions were observed. Furthermore, maximum adsorption was recorded at pH 5 and when pH was increased above this point adsorption capacity decreased and point of zero charge was found to be at pH 8. The catalyst surface was positively charged during the reaction, therefore, experiencing high affinity for anions or ionized compounds. Similarly, Guo and Al-Dahhan (2003) studied the effect of pH between 3.9-5.1 in a basket stirred tank reactor over Al-Fe pillared clay catalyst. They studied phenol oxidation using two solutions; in the first solution, pH was adjusted using sulfuric acid whereas in the second solution pH was not adjusted. It was reported that when pH was adjusted, phenol removal rate

was 2 times higher compared to when pH was not adjusted and 100 % conversion was achieved at pH 3.9. Yadav et al., (2016) studied the effect of pH between 2.8 -8 in a batch reactor using Fe supported on carbon-containing nanoparticle catalysts. During phenol oxidation, a decrease in pH from 6 to 2.8 was observed indicating the formation of carboxylic acids and 100 % conversion was achieved at pH 2.8 after 210 min. However, for safety reasons they adjusted the pH to 8 using KOH so that the final pH of the solution after oxidation will be ca.5 and the oxidation rate remained the same when compared with the first experiment without pH adjustment and complete removal of phenol was achieved at the same reaction time of 210 min.

In summary, the studies indicate that the system performs better when the solution is acidic. However, acidic solutions are highly corrosive and can damage the reactor, thus necessitating the use of corrosion-resistant materials during reactor design (Resende et al. 2018). Moreover, at low pH most catalysts are leached increasing the cost of the catalyst. It is therefore advisable to invest in the development of a catalyst that will reduce phenol directly to inorganic compounds without the formation of carboxylic acids to avoid low pH values in the reactor.

2.3.4. Effect of liquid and gas hourly space velocity

Liquid hourly space velocity (LHSV) has a negative impact on phenol conversion. This is due to the fact that an increase in LHSV reduces space-time resulting in less contact time between the phases. An increase in LHSV also increases film thickness and liquid holdup which decreases contact time between gas and liquid on the catalyst active sites therefore resulting in high resistance to mass transfer. However, the effect of gas flow is the opposite of LHSV with an increase in gas flow resulting in improved phenol removal due to decreased film thickness, liquid holdup and enhanced mass transfer. Abid et al., (2016) investigated the effect of both liquid and gas flow rates on phenol oxidation using a trickle bed reactor over activated carbon catalyst. They studied liquid flow rate of 1.662, 0.996 and 0.6 ml/min while gas flow rates were 10, 20, 30 and 60 ml/min. According to their observation, an increase in LHSV has a negative influence on phenol conversion with 79 % reached at 1.662 ml/min while 86.8 % and 95.6 % were reached when LHSV was decreased to 0.996 and 0.6 ml/min. Furthermore, phenol removal reached 79.7 %, 82.5 %, 86.8 % and 83.5 % at gas flow rate of 10, 20, 30 and 60 ml/min, respectively. The maximum conversion was reached at 30 ml/min of gas flow due to the decrease in film thickness and liquid holdup, whereas the decrease in conversion at 60 ml/min was due to a decrease in wetting of the catalyst surface caused by liquid mal-

distribution. Similarly, Mohammed et al., 2016 investigated the effect of liquid and gas flow on phenol oxidation in a trickle bed reactor using 0.48 % Pt/ γ-Al_2O_3 catalyst operated in the following gas flow, 20, 40, 80 and 100 % and liquid hourly space velocity between 1, 2 and 3 h^{-1}. The maximum conversion was reached at a gas flow rate of 80 % and a further increase in gas flow resulted in a slight decrease in conversion due to the decreased spreading of the liquid film. In their study Mohammed, 2014 studied the effect of gas and LHSV in a trickle bed reactor that was operated between (60-100 %) stoichiometric oxygen excess (S.E) and LHSV ranging from 1, 2 and 3 h^{-1} over activated carbon catalyst. It was reported that maximum conversion was achieved when the gas flow rate was 80 % S.E and when the flow rate was increased beyond this point, conversion was decreased due to the decreased. However, phenol conversion increased with a decrease in LHSV and the following results were reported when LHSV was 2 and 3 h^{-1}, 87.16 and 82.5 %.

It can be concluded that an increase in gas flow has a positive influence whereas, LHSV has a negative impact. A prior knowledge of the flow regime is required to choose the correct design equation for TBR. Moreover, hydrodynamics and transport properties of the system can change dramatically between the flow regimes impacting final results significantly. Currently, empirical flow map or relationships are used to predict the flow patterns and there is a limited theoretical foundation developed to predict the transition between the flow regimes. On the other hand, an increase in computing memory and technological advances saw an increase in the use of CFD and Tomography to understand the flow transition between the regimes. For developing countries with limited resources, CFD is the cheapest technique that can be used to understand the interaction between the phases.

2.4. Kinetic Model

Kinetics models are crucial for the design and up-scaling of laboratory reactors to industrial reactors (Zarca et al, 2015). A simple power-law model can be used to determine the rate of reaction in a trickle bed reactor as reported by (Eftaxias, 2002; Eftaxias et al., 2005; Abid et al, 2014; Abid et al, 2016, Makatsa *et al.*, 2019). The simple power law can be expressed as follow:

$$-r_{ph} = k_{oi}.Exp\left[{}^{-E_{ai}}/_{RT}\right].C_i.{x_{O_2}}^{\alpha} \qquad (11)$$

Where, $-r_{ph}$ is reaction rate, k_{oi} is a frequency factor, E_{ai} is activation energy, *R* is ideal gas constant, *T* is temperature, x_{O_2} is dissolved molecular oxygen mole fraction, α is reaction order with respect to oxygen concentration and C_i is phenol concentration.

Abid et al, 2016 used a different catalyst and slightly higher temperature compared to their previous study (Abid et al, 2014). In this study, they used activated carbon as a catalyst and the reactor was operated between temperatures of (120 °C – 160 °C) and pressure of 2 to 9 bar. The activation energy was a bit higher (77.7 KJ/mol) and the reaction order with respect to oxygen was 0.6. Abid et al, 2014 also used a power-law model to determine reaction rate parameters using 0.5 % Pt/γ-Al_2O_3 catalyst in a trickle bed reactor operated between 85 – 140 °C and pressure of 1 to 6 bar. Oxygen reaction order was found to be 0.69 and activation energy was 29.3 KJ/mol. Similarly, Eftaxias et al., 2005 used power law model to determine reaction rate parameters over activated carbon (AC) catalyst in a trickle bed reactor operated between temperatures of 120 – 160 °C and pressure of 1 and 2 bar. The kinetic model was able to adequately predict phenol conversion only when the conversion was below 70 % and for conversions above 70 %, the model overestimated experimental conversion. The deviation was attributed to liquid maldistribution reinforced by the smaller reactor configuration. Furthermore, phenol oxidation activation energy over the catalyst was found to be 69, 3$\pm$0.4 KJ/mol and the oxygen mole fraction was 1,015$\pm$0.02. Eftaxias, 2002 used both power-law and Langmuir-Hinshelwood (L-H) model in a trickle bed reactor operated between temperatures of (120 °C – 160 °C) and pressure of 6 to 12 bar over two catalysts (CuO/γ-Al_2O_3 and AC). It was reported that when power law model was used in the presence of CuO catalyst; phenol and acetic acid were estimated very well, however, the model failed to predict the remaining carboxylic acids and quinone-like compounds. In addition, L-H model was not used for phenol oxidation because preliminary experiments obtained from adsorption experiments indicated that phenol was not adsorbed on the surface of the catalyst. The reaction activation energy was found to be 74.9 KJ/mol and the oxygen order was 0.311. In contrast, when the AC catalyst was used, phenol destruction activation energy was slightly lower (70.3$\pm$0.4 KJ/mol) and reaction order with respect to oxygen was 0.95$\pm$0.02.

Another model that is commonly used to correlate adsorption-desorption of heterogeneous catalysts is Langmuir-Hinshelwood (L-H) or Langmuir-Hinshelwood-Hougen-Watson (LHHW) reported by (Eftaxias et al., 2001, 2006; Guo and Al-Dahhan, 2003; Wu et al, 2005). Langmuir-Hinshelwood (L-H) model can be expressed as follows:

$$r_i = k_{ap,i} \frac{K_i C_i}{1+\sum_j K_j C_j} \quad (12)$$

Where r_i is reaction rate, $k_{ap,i}$ is reaction kinetics constant, K_i and K_j are adsorption constants, C_i and C_j are species concentrations.

Eftaxias et al., 2001 used the L-H model to determine kinetics parameters using a copper-based catalyst (CuO/ γ-Al_2O_3) with the temperature of the reactor between 120 °C – 160 °C. They reported activation energy of 74.9 KJ/mol and an oxygen reaction order of 0.31. Table 2 summarizes kinetic models used by Guo and Al-Dahhan, 2003 in a basket stirred tank reactor operated between 90 and 150 °C over Al-Fe pillared clay catalyst whereas Table 3 give a summary of activation energies and reaction conditions. The power-law model (M1) is used to correlate the simplest form of the surface reaction rate. As can be seen from the reaction mechanism of model M2, adsorption and desorption of phenol and oxygen take place on the same site and a more complex model like LHHW is used to model the process. The mechanism of M3 is similar to M2 because of single-site adsorption. In contrast to M2, oxygen molecules dissociate to allow surface reaction of physically adsorbed phenol and oxygen to take place. The last model M4 is completely different from previous models because dissociated molecules are adsorbed on two active sites. To check the quality of the models, they were compared with experimental data. Parity plot was used to compare experimental results with calculated results and experimental data was adequately fitted when kinetic model M2-M4 was used whereas M1 under predicted phenol of high concentration. When model M4 was used, the activation energy of 34.29 KJ/mol was reported.

Table 2: Kinetic models proposed for heterogeneous CWAO reaction(Guo & Al-Dahhan 2003).

Kinetic Model	Equation	Mechanism
M1	$r_H = k_1[A]^p[O_2]^q$	Empirical Approach
M2	$r_H = \frac{k_1 K_A K_{O_2}[O_2][A]}{(1+K_A[A]+K_{O_2}[O_2])^2}$	Single site $O_2 + * \leftrightarrow O_2*$
M3	$r_H = \frac{k_1 K_A K_{O_2}^{0.5}[A][O_2^{0.5}]}{(1 + K_A[A] + K_{O_2}^{0.5}[O_2^{0.5}])^2}$	Single site $O_2 + 2^* \leftrightarrow 2O^*$
M4	$r_H = \frac{k_1 K_A K_{O_2}^{0.5}[A][O_2^{0.5}]}{(1 + K_A[A] + K_{O_2}^{0.5}[O_2^{0.5}])}$	Dual Sites $O_2 + 2^* \leftrightarrow 2O^*$

*Represent the reactant on the catalyst active site

Eftaxias et al., 2006 used L-H model to determine the kinetic parameters using an active carbon catalyst with the temperature of the reactor between 120 °C – 160 °C and pressure of and 1 to 2 bar. The oxidation of phenol to 4-HBA and p-benzoquinone were found to be 82.4 and 72 KJ/mol whereas oxygen reaction orders were, 1.02$\pm$ 0.02 and 0.92$\pm$0.01, respectively. Similarly, Wu et al, 2005 used an L-H model to predict kinetics parameter using copper supported on activated carbon catalyst with the reactor operated between 140 °C – 160 °C. The activation energy was found to be 35.4 KJ/mol and first order reaction for phenol was assumed.

Table 3: Activation energies and reaction orders found in literature using different reactors.

Catalyst	Reactor	Model Equation	Temperature (°C)	Activation Energy(KJ/mol)	Oxidant Reaction Oder	Ref
CuO/ γ-Al_2O_3	TBR	$r_i = K_{ap,i}\frac{K_i C_i}{1+\sum_j K_j C_j}$	120-160	74.9	0.31	(Eftaxias *et al.*, 2001)
Al/Fe pillared clay	BSTR	$r_H = \frac{k_1 K_A {K_{O_2}}^{0.5}[A]{C_{O_2}}^{0.5}}{1+K_A[A]}$	190-150	34.29	-	(Guo and Al-Dahhan, 2003)
AC	TBR	$r_i = k_{oi}\exp(\frac{-E_{ai}}{RT}){x_{O_2}}^{\alpha}\frac{K_{Oi}\exp(-\frac{\Delta H_i}{RT})C_i}{1+\sum K_{Oj}\exp(-\frac{\Delta H_j}{RT})C_j}$	120-160	82.4 and 72	1.02± 0.02 and 0.92±0.01	(Eftaxias *et al.*, 2006)
Cu/AC	BSTR	$r_H = K_{het,app}\frac{C_A C_B}{(1+K_A C_A)^{2,0}}$	140-160	35.4	-	(Wu et al., 2005)

A complete reduction of phenol to CO_2 and H_2O is very complex and its reaction mechanism is not yet fully understood. Some oxidation by-products are as toxic as phenol and therefore, kinetic models accounting for all intermediates are very important. Most studies show that the power law model can be used to predict phenol. However, this model has limitations because it can't be used when phenol and its intermediates are adsorbed on the surface of the catalyst. As shown in Table 2, mathematical correlations (M2-M4) can be used to account for adsorption and desorption of the organic pollutant on the surface of the catalyst. In conclusion, L-H model is the most suitable kinetic model for the oxidation of phenol and its intermediates.

2.5 CFD Modelling

The use of TBR in heterogeneous catalysis is common, especially when gas and liquid react to form products. However, most studies are conducted in a laboratory fixed bed reactors and the scaling up of these reactors to industrial reactors is problematic due to complex interactions of fluid dynamics with reaction kinetics. Moreover, the change in hydrodynamic parameters is significant when laboratory reactors are scaled up to commercial reactors and correlations developed in a laboratory reactor might not work. Ranade and Gunjal (2011) suggested that the scale of the reactor affects its performance. In addition, these authors listed several factors that are directly affected during reactor scaling-up as follows; reactor to particle diameter ratio, reactor volume, bed porosity, wetting, channelling, liquid mal-distribution, dispersion and reactor operating mode (isothermal/adiabatic). Moreover, these researchers concluded that wall effect is predominant in laboratory TBR whereas flow mal-distribution is common in industrial TBR due to large bed diameter. On the other hand, when CFD model is developed correctly, it should be independent of the scale of the reactor because these models are based on conservation of mass, energy and momentum. CFD simulations provide a time saving and cost-effective approach in the reactor design. In a typical design, the software is used to solve a system of complex mathematical equations (Haro et al., 2016). The software can be used to solve multiple phase flows like gas-liquid, liquid-solid and gas-solid flows (Kapfunde et al., 2018, Makatsa et al., 2020). Multi-phase flow systems can be modeled in three different ways using volume of fluid (VOF), Eulerian–Lagrangian and Eulerian–Eulerian approach. The first method (VOF) is the easiest and all phases are considered as a non-interpenetrating continuum. The method solves

a single set of momentum equations and tracks the volume of all phases in a computational domain. The method is suitable for analysis of multiple phase systems of the small domain and modeling the behavior of the interface. In addition, the method is used mostly when modeling large scale systems. The Eulerian–Lagrangian method considers a fluid phase as a continuum and solves a system of Navier–Stokes equations for the continuous phase while solving the dispersed phase by tracking the particles through the calculated flow field. This model is recommended for modeling of the multi-phase flow with less volume fraction of the dispersed phase and for modeling liquid fuel and spray dryers. In contrast, the Eulerian-Eulerian method is based on the assumption that every phase is an interpenetrating continuum. The method uses the approach of single pressure for all phases. Governing equations are solved separately for each phase (continuity, momentum, energy, and species transfer equations). This approach is suitable for modeling of the multi-phase flow with volume fraction ranging from 0 to 1 and for multiple phase reactors with more than one dispersed phase (Mousazadeh 2013).

Ranade et al., (2011) used a model developed by Attou and Ferschneider (1999) to simulate the flow regime where the liquid flow was in the form of droplets. Mousazadeh (2013) used CFD to predict the formation of hot spots in a trickle bed reactor. A hot spot was observed when there was a local blockage preventing the fluid from flowing. Furthermore, there was a temperature difference of 153 °C between the hot spot and the surrounding area. It was concluded that the hot spots were formed when liquid cannot convect in the radial or axial direction. Lopes and Quinta-Ferreira (2007) developed a computational fluid dynamics model of a trickle bed reactor operated between the temperature of 170 °C – 200 °C and pressures of 10 – 30 bar. These authors used FLUENT 6.1 and Euler–Euler multi-phase flow approach to model the behavior of the fluid inside the reactor. Furthermore, the researchers studied the influence of gas and liquid flow rate within the trickle flow regime ranging between (gas: 0.10 – 0.70 and liquid: 0.5 – 5 kg/m^2s). In order to validate their findings for pressure drop and liquid holdup, a spherical catalyst of a 2 mm diameter was used as a reactor packing. In addition, they mapped both gas and liquid flow; and found maximum velocities to be 0.5 and 0.005 cm/s respectively. Their results showed that the reactor was operated within a trickle flow regime. According to their findings, an increase in liquid mass flux resulted in an increase in liquid holdup whereas an increase in pressure resulted in a significant decrease of the liquid holdup. The increase in liquid mass flux improves interaction between gas and liquid which causes turbulence and thickens the

liquid film. These changes resulted in an increase in liquid side shear stress due to high-pressure drop and resistance became more pronounced in comparison to the driving force. Their results were in agreement with (Beni & Khosravi-Nikou 2015; Mousazadeh 2013; Kuzeljevic 2010). The researchers concluded that a change in reactor pressure is more pronounced on pressure drop than liquid holdup. Similarly, Beni and Khosravi-Nikou (2015) modeled hydrodynamics of the trickle bed reactor and used 300 spherical particles arranged in a hexagonal pattern with maximum space between them, not exceeding 3 % of particle diameter. They simulated only 12 layers due to computational limitation and investigated the effect of pressure on hydrodynamics parameters at lower pressures ranging between (0.1, 0.5 & 1 MPa). They also varied gas and liquid superficial velocities between (0.086 & 0.25 m/sec) and (<0.005-0.03 m/s) respectively. Regardless of mild pressure they also reached the same conclusion as (Lopes & Quinta-Ferreira 2007).

Accurate estimation of hydrodynamic parameters is an important step for reactor design and performance evaluation of the catalyst. The complex internal bed structure and phase interaction are the controlling factor in TBR. Hydrodynamics are affected by; particle properties, packing characteristics of the bed and operating conditions. There are methods and correlations available for determining hydrodynamic parameters such as liquid holdup, axial dispersion and CFD.

In summary, CFD can be used to model liquid mal-distribution and predict the formation of hot spots. Hot spots are undesired because they may reduce production by deactivating the catalyst or decrease the mechanical strength of the wall. It is recommended that a simulation of TBR fitted with a mechanical liquid distributer at the top be simulated.

Chapter 3: Experimental Methods

3.1 Materials

The pillaring agent was prepared from sodium hydroxide (NaOH)**,** anhydrous aluminum nitrate $Al(NO_3)_3 \cdot 9H_2O$, and zirconium chloride ($ZrOCl_2 \cdot 8H_2O$) which were purchased from Merck Chemicals (Pty) Ltd. Natural bentonite clay used in this study was obtained from ECCA Holdings (Pty) Ltd. Oxalic acid used for monolith acid treatment and silver nitrate ($AgNO_3$) were bought from Sigma-Aldrich Chemical Co. High purity water used to prepare solutions was taken from Mintek laboratories. Cordierite monolith used as support was purchased from Ghophin Chemical. All chemicals used in this study were used as received without modification.

3.2 Catalyst Preparation

A pillaring solution was prepared by mixing 83.3 mL of 0.1 M $ZrOCl_2 \cdot 8H_2O$ with 250 mL 0.1 M $Al(NO_3)_3 \cdot 9H_2O$. In addition, a solution of 0.1 M NaOH was added dropwise to the mixture prepared while stirring. After the complete addition of NaOH, the solution was stirred for another 2 h at room temperature followed by ultrasonication for 10 min at 25 °C. To prepare pillared clay catalyst, dry bentonite clay was added to the pillaring solution and the resulting slurry was stirred at room temperature for 30 min followed by ultrasonication for 10 min at 25 °C. After sonication, the slurry was centrifuged for 8 min and the supernatant was discarded. The sediment was washed with high purity water to remove any excess chlorides followed by oven drying at 120 °C for 16 h. The oven-dried sample was calcined at 400 °C for 2 h.

3.3 Acid treatment of cordierite monolith

Before wash coating, honeycomb cordierite monoliths were acid treated with 20 % (w/v) oxalic acid. The cordierite monoliths were immersed in the acid for 8 h to remove impurities and improve surface area. This was followed by thoroughly washing of the monoliths with high purity water. After washing, the monoliths were oven-dried at 120 °C for 16 h followed by calcination in a muffle furnace at 500 °C for 2 h.

3.4 Wash-coating of cordierite monolith with Al/Zr-PILCs

The pillared clay catalyst prepared in the previous step was milled for 90 min in the Netzsch-Feinmahltechnik GmbH LME1 wet grinding ball mill using ceria-zirconia beads as the grinding media. This was done to achieve a particle size of 2-5 μm. The beads were separated from the slurry using fluidization. Excess water was decanted, the sample was then dried overnight at 120 ℃. The wash-coating slurry was prepared using the milled pillared clay catalyst, high purity water, 10 wt. % silica solution and glycerol in a ratio of (1:2:1.5:2).

Glycerol was used as a dispersant to ensure the wash-coat dries homogenously and silica was used as a binding agent, to increase the adhesion of the wash-coat onto the surface of the monolith. Four wash-coated monolith samples were prepared by dip-coating the monoliths in the slurry three times, with an immersion time of 5 min per dip. The resulting samples were then dried, two of which were dried in the oven at 40 ℃ and 60 ℃ for 30 min whereas the other two were dried using thermally assisted microwave oven at 80 ℃ for 30 min and the other one was dried at room temperature for six weeks. The dry samples were then calcined at 500 ℃ for 2 h.

3.5 Characterization techniques

The X-ray diffraction (XRD) patterns were attained using a Bruker AXS D8 X-ray advanced powder diffractometer equipped with CoKα-radiation, over a 2θ range from 5 to 80° at 40kV and 40mA with stepwise angle increment of 0.02°/s. The morphology of the wash-coated monolithic catalyst was determined using Zeiss EVO MA15 scanning electron microscopy, with a magnification of 20 µm. Micromeritics Tristar 3000 instrument was used to determine the surface area of the catalyst. N_2 adsorption-desorption isotherm experiment was conducted at -196 ˚C using liquid nitrogen. Prior to the experiment the sample was degassed at 150 ˚C under vacuum for 4 h.

3.6 CWAO Experiment

Phenol oxidation experiments were conducted in a stainless steel TBR of 56 mm diameter and 430 mm length shown in Figure 28 (Appendix A). The pollutant (phenol) was measured using Shimadzu HPLC equipped with UV detector at wavelength of 210 nm. A mobile phase of (65/35) % methanol in water was used and injected at 5µL, whereas the flow rate was set to 1 ml/min. A C18 (Waters spherisorb S5ODS2) column 25 cm x 4.6 mm x5 µm was used as a stationary phase. Before the reaction start, the pump and mass flow controller were both

calibrated and the calibration curves are shown in Figure 25 and 26 in the appendix A. In addition, a standard solution of phenol was ran to determine retention time and the results can be found in appendix A (Figure 27). Catalyst activity was tested at 160 ˚C, 10 bar over Al/ Zr-PILC catalyst and the reaction was stopped after 3 hrs.

3.7 Computational fluid dynamics model

3.7.1 Governing equations

A multiphase Eulerian CFD model of phenol oxidation in a TBR was developed using a commercial software Fluent 2019R2. The following set of mathematical equations are incorporated into a CFD code solver.

Mass conservation equation:

$$\frac{\partial_{\varepsilon_k \rho_k}}{\partial t} + \nabla . \varepsilon_k \rho_k U_k = 0 \quad (12)$$

Momentum conservation equation:

$$\frac{\partial(\varepsilon_k \rho_k U_k)}{\partial t} + \nabla . (\varepsilon_k \rho_k U_k U_k) = -\varepsilon_k \nabla P_k + \nabla . (\varepsilon_k \mu \nabla U) + \varepsilon_k \rho_k g + F_{K,R}(U_k - U_r) \quad (13)$$

Where ε_k is volume fraction for each phase, ρ_k is the density of the k-th phase, U_k is the cell velocity of the k-th phase and $F_{K,R}$ is an interphase momentum exchange (Ranade et al., 2011). The interface coupling term $F_{K,R}$ can be expressed as follow

$$F_{GL} = \varepsilon_G \left(\frac{E_1 \mu_G (1-\varepsilon_G)^2}{\varepsilon_G{}^2 d_P{}^2} \left[\frac{\varepsilon_S}{(1-\varepsilon_G)}\right]^{0.667} + \frac{E_2 \rho_G (U_G - U_L)(1-\varepsilon_G)}{\varepsilon_G d_p} \left[\frac{\varepsilon_S}{(1-\varepsilon_G)}\right]^{0.333}\right) \quad (14)$$

$$F_{GS} = \varepsilon_G \left(\frac{E_1 \mu_G (1-\varepsilon_G)^2}{\varepsilon_G{}^2 d_P{}^2} \left[\frac{\varepsilon_S}{(1-\varepsilon_G)}\right]^{0.667} + \frac{E_2 \rho_G U_G (1-\varepsilon_G)}{\varepsilon_G d_p} \left[\frac{\varepsilon_S}{(1-\varepsilon_G)}\right]^{0.333}\right) \quad (15)$$

$$F_{LS} = \varepsilon_L \left(\frac{E_1 \mu_G \varepsilon_S{}^2}{\varepsilon_G{}^2 d_P{}^2} + \frac{E_2 \rho_L U_G \varepsilon_S}{\varepsilon_L d_p}\right) \quad (16)$$

Where F_{GL}, F_{GS}, F_{LS} are gas-liquid, gas-solid and liquid-solid momentum exchange terms. To understand turbulence inside the reactor standard k-ε model was chosen and the software solved the following mathematical equations (Lopes & Quinta-Ferreira, 2010);

$$\mu_{t,L} = \rho_L C_\mu \frac{k_L^2}{\varepsilon_L} \tag{17}$$

The liquid viscosity turbulence $\mu_{t,L}$ is calculated from the transport equations by determining kinetic (k_L) and dissipation energy (ε_L) from the following equations (Lopes & Quinta-Ferreira 2007)

$$\frac{\partial}{\partial t}(\rho_L \alpha_L k_L) + \nabla.(\rho_L \alpha_L \vec{u}_L k_L) = \nabla.\left(\alpha_L \frac{u_{t,L}}{\sigma_k} \nabla k_L\right) + \alpha_L G_{k,L} - \alpha_L \rho_L \varepsilon_L + \alpha_L \rho_L \Pi_{k,L} \tag{18}$$

$$\frac{\partial}{\partial t}(\rho_L \alpha_L \varepsilon_L) + \nabla.(\rho_L \alpha_L \vec{u}_L \varepsilon_L) = \nabla.\left(\alpha_L \frac{u_{t,L}}{\sigma_\varepsilon} \nabla \varepsilon_L\right) + \alpha_L \frac{\varepsilon_L}{k_L} \times (C_{1\varepsilon} G_{k,L} + C_{2\varepsilon} \rho_L \varepsilon_L) + \alpha_L \rho_L \Pi_{\varepsilon,L} \tag{19}$$

The following parameters were taken as constants C_μ, $C_{1\varepsilon}$, $C_{2\varepsilon}$, σ_k, σ_ε and assigned the following values 0.09, 1.44, 1.92, 1.0 and 1.3, respectively. Enthalpy was calculated from conservation of energy in a multiphase Eulerian model as follows (Manoharan & Buwa 2019; Lopes & Quinta-Ferreira 2007).

$$\frac{\partial}{\partial t}\left(\rho_q \alpha_q h_q\right) + \nabla.\left(\rho_q \alpha_q \vec{u}_q h_q\right) = -\alpha_q \frac{\partial p_q}{\partial t} + \bar{\bar{\tau}}_q : \nabla \vec{u}_q - \nabla.\vec{q}_q + S_q + \sum_{p=1}^{n} (\vec{Q}_{pq} + \dot{m}_{pq} h_{pq} - \dot{m}_{qp} h_{qp}) \tag{20}$$

The specific enthalpy of phase q is represented by h_q and $\vec{q}_q$ is a heat flux. The heat exchange intensity between the q and p phases is represented by $\vec{Q}_{pq}$ whereas interphase enthalpy is represented by h_{pq} and S_q is the source term. By activating species transport the solver modeled volumetric reaction using the following equation (Lopes & Quinta-Ferreira 2010):

$$\frac{\partial \alpha_q \rho_q C_{q,i}}{\partial t} + \nabla.\left(\alpha_q \rho_q u_q C_{q,i}\right) = \nabla.\left(\alpha_q \rho_q D_{q,i} \nabla C_{q,i}\right) + \alpha_q \rho_q S_{q,i} \tag{21}$$

3.7.2 Mesh

ANSYS mechanical 2019R2 was used as a meshing tool and iterations were based on 3263050 elements and 691327 nodes. Figure 8 shows a mesh of the reactor and a monolith.

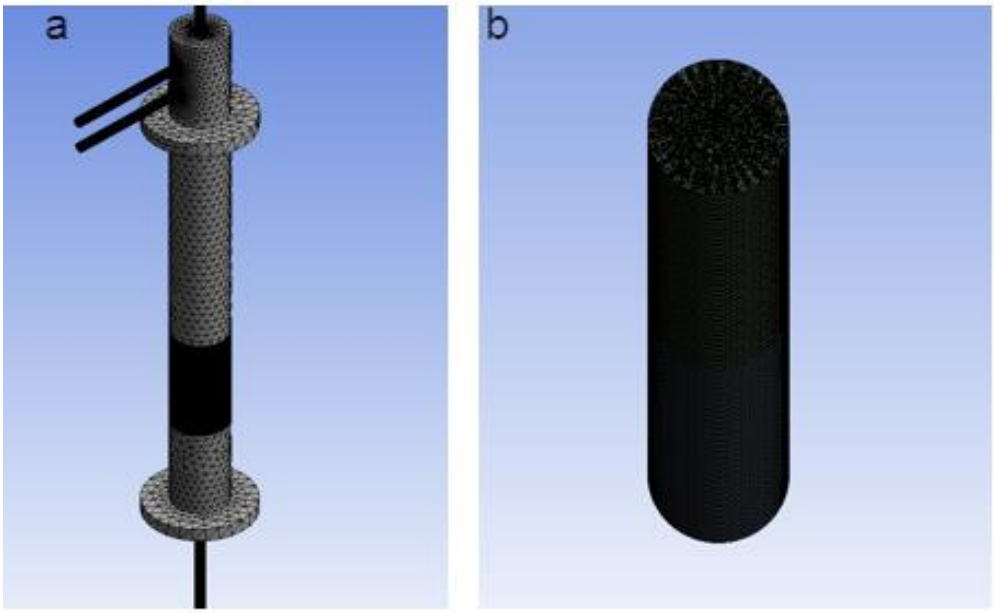

Figure 8: 3D reactor geometry and mesh structure of (a) TBR and (b) monolith.

3.7.3 Boundary conditions

A three dimensional (3D) model was developed using commercial software and conservation of mass, momentum, energy and species transport equations were solved. The reactor bed was packed with silica and the velocity profile of the packing was fixed to zero. The inlet velocities of phenol and gas are listed in table 4. The linearization error was minimized by calculating aggregate imbalances and setting the tolerance to 10^{-6} in the residuals and discretization error accuracy was set to second order.

Table 4: Reactor dimensions and operating conditions

Reactor diameter	0.056 m
Reactor length	0.43 m
Particle diameter	0.002 m
Porosity	0.63
Pressure	10 bar
Temperature	433 K
Gas flow rate	0.012 m/s
Liquid flow rate	0.00007 m/s
Activation energy	42289 J/kg.mol
Pre-exponential factor	248948.2

Chapter 4: Results and Discussion

4.1 Characterization of the catalyst

Figure 9 shows the X-ray diffraction (XRD) patterns of natural and pillared bentonite clay. Successful pillaring of bentonite is confirmed by a shift of Na-montmorillonite peak from 8.25° to a lower angle of 7° and an increase of basal spacing (d_{001}) from 12.44 to 15.15 Å confirming intercalation of bentonite by metal oxides. Moreover, the structure of natural bentonite remained the same even after the pillaring process as can be confirmed by unchanged peaks observed after pillaring.

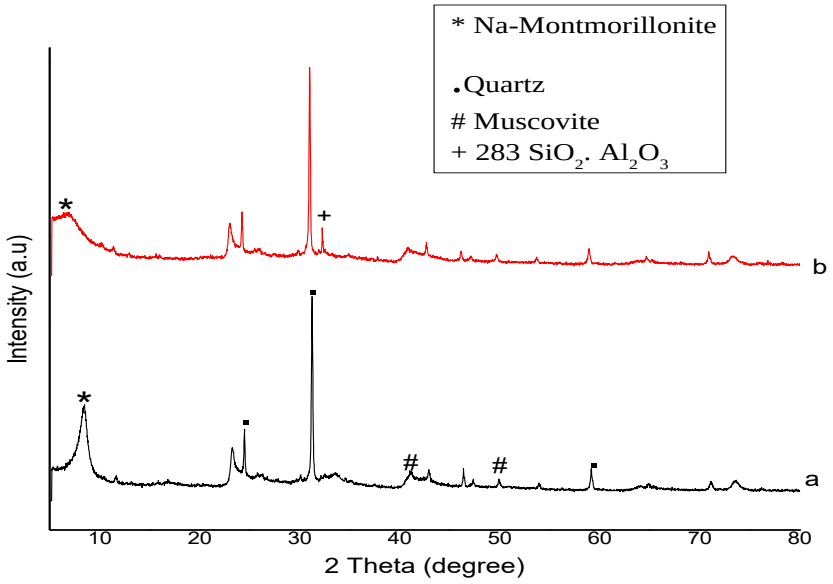

Figure 9: XRD patterns of (a) Natural bentonite clay (b) Al/Zr pillared clay catalyst.

Cordierite monolith diffraction peaks usually contain aluminum oxide (Al_2O_3), silicon dioxide (SiO_2) and magnesium oxide (MgO). During acid treatment aluminum (Al) and magnesium (Mg) species are leached (Adamowska & Costa 2014). Figure 10 shows peaks of the bare monolith, pretreated and wash coated cordierite. The peaks observed are consistent with XRD standard PDF card no. 089-1487 for cordierite reported by (Adamowska & Costa., 2014; Soghrati et al., 2014). After acid and thermal treatment, the cordierite peaks did not disappear. However, the intensity of the peaks decreased indicating leaching of Al and Mg species (Adamowska & Costa., 2014). Furthermore, new peaks of spinel ($MgAl_2O_4$) were observed at 29, 43° and the

results are consistent with findings of Soghrati *et al.*, (2014). On the other hand, the intensity of the SiO_2 peak observed at 11.9° increased due to excess silica added during the wash-coating process. Moreover, corundum (α-Al_2O_3) peaks appeared at 29.9, 41, 44, 50.9, 61.8, 67.8, and 78.9° and this type of aluminum is known to facilitate anchoring of the catalyst (Baloyi et al, 2018d). In addition, bentonite peak is not observed in the XRD pattern after wash coating the monolith due to the low content of sodium (Na). This concept is further supported by EDS results of Al/Zr-PILCs (3:1) reported by Baloyi et al., (2018c). In their study, Na content decreased from 3.73 to 0.26 % for bentonite and Al/Zr-PILCs (3:1), respectively. On the other hand, Elmer (2008) reported the presence of amorphous silica on the surface of the cordierite after thermal treatment and this can be the reason why the peak is not observed.

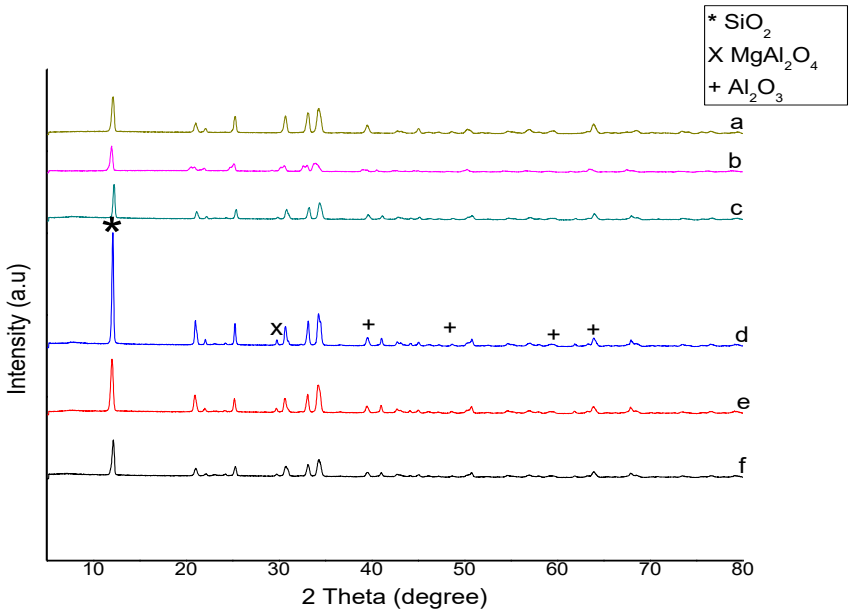

Figure 10: XRD patterns of (a) Bare monolith, (b) monolith acid treated with oxalic acid and calcined at 500 °C for 2 h, (c) Al/Zr-PILCs monolith dried at 60 °C, (d) Al/Zr-PILCs monolith dried at 40 °C, (e) Al/Zr-PILCs monolith microwave dried, (f) Al/Zr-PILCs monolith dried at room temperature for six weeks.

Acid treatment targets alumina and magnesia species available on the surface of cordierite monolith. After acid treatment and calcination, the surface of the monolith becomes rough leaving microporous silica. In addition, a layer of α-Al_2O_3 develops on the edges of the monolith as seen in Figure 11(b). Moreover, a thick layer of silica is deposited on the corners of the monolith after wash coating as seen in Figure 11(d) and zirconia is also highly concentrated on

the edges of the structure as seen in 11(c). Furthermore, Mg concentration is significantly increased on the surface of the structure as seen in Figure 11(d) and this increase is attributed to the layer of the catalyst deposited on the surface of the support. Baloyi et al., (2018c) reported that Al/Zr-PILCs (3:1) catalyst contains 1.29 % of Mg species.

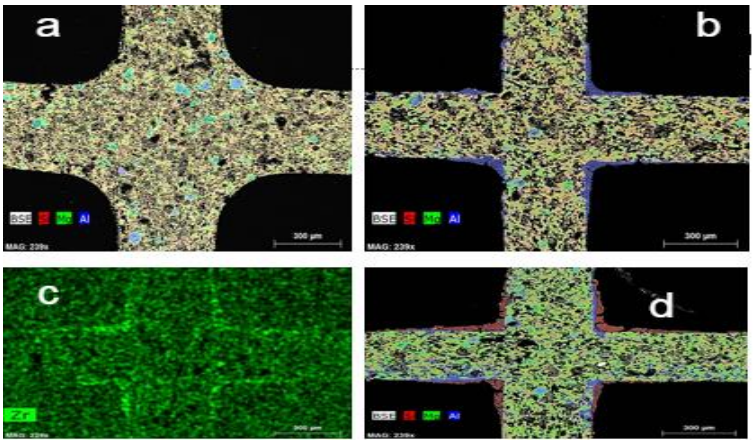

Figure 11: Cross-section SEM images of the bare monolith (a), monolith acid treated with oxalic acid and calcined at 500° C for 2 h (b) zirconium mapping image (c) and wash coated monolith (d).

After acid treatment, the macro-pores on the surface of the cordierite become bigger indicating good anchoring property of the support (Villegas et al., 2007). Figure 12(c) shows that the catalyst is uniformly distributed on the surface of the cordierite. As seen in Figure 12(c-d) the morphology of the coating is interpreted by the oxide layer (intense red indicating SiO_2) generated on the surface of the cordierite and the presence of zirconia.

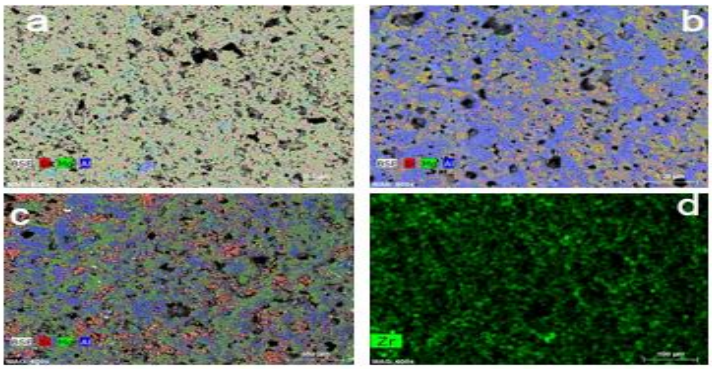

Figure 12: Backscattered electron x-ray mapping images were taken on the surface of the bare monolith (a), monolith acid treated with oxalic acid and calcined at 500° C for 2 h (b), wash coated monolith (c), and zirconium mapping image (d).

As seen in Figure 13 acid pretreatment makes the surface rough and exposes a layer of α-Al_2O_3 which facilitate binding of the active catalyst. Figure 13 (c-d) show wash coated monolithic catalyst and in all images, no cracks are observed. This can be attributed to glycerol since it is used as a retardant to control the evaporation rate. Glycerol is known to contain three hydrophilic alcoholic hydroxyl groups responsible for its hygroscopic nature (Pagliaro et al., 2008). Therefore, glycerol absorbs additional water present in the sample and ensures that drying does not occur rapidly. However, the microwave sample depicts a smoother coating. This is due to homogenous heat dispersal by microwaves during drying (Villegas et al., 2007).

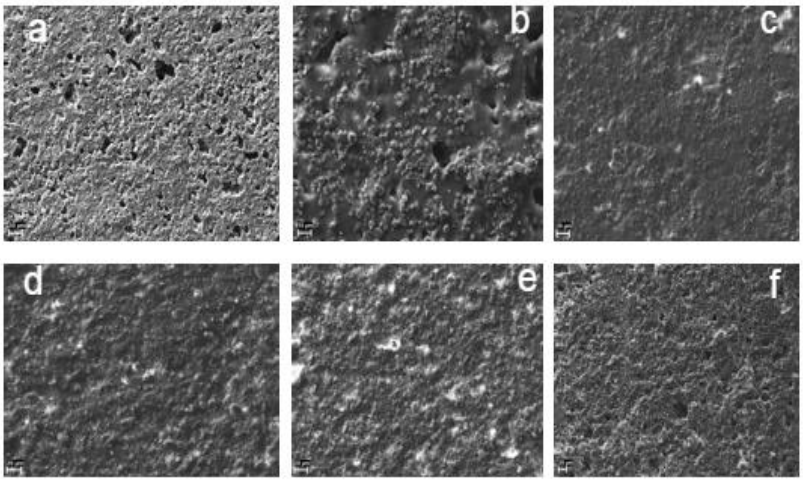

Figure 13: Secondary electron images were taken on the surface of bare monolith (a), monolith acid treated with oxalic acid and calcined at 500° C for 2 h (b), wash coated and microwave dried (c), wash coated and oven-dried at 40° C (d), wash coated and oven-dried at 60° C (e) and wash coated and dried at room temperature (f).

Table 5 lists the textural properties of the materials tested and it is evident that after acid treatment the surface area, pore volume and diameter increased. Soghrati *et al.*, (2014) claimed that this increase is due to the formation of meso and micropores on the surface of the monolith during acid treatment. Furthermore, natural bentonite surface area increased from 61 to 103.9116 m^2/g due to increased pore volume (Moma et al., 2018).

Table 5: BET results of the catalyst and support.

Sample	S_{BET} (m^2/g)	V_{pore}(cm^3/g)	d_{pore}(nm)
Bentonite	61	0.11	15.31
Al/Zr-PILC	103.9116	0.21	2.1
Bare monolith	0.16	0.0002	4.82
Acid treated monolith	19.2426	0.037338	4.94

4.2 Catalyst activity test

Figure 14 shows phenol conversion with time when Al/Zr pillared clay catalyst was used. The maximum conversion (100 %) was reached after 3 h and this increase can be attributed to the increase in the number of active sites available on the catalyst surface. Similar results were reported by (Baloyi et al., 2018c; Moma et al., 2018) when they studied the removal of phenol by CWAO using Al/Zr-PILCs.

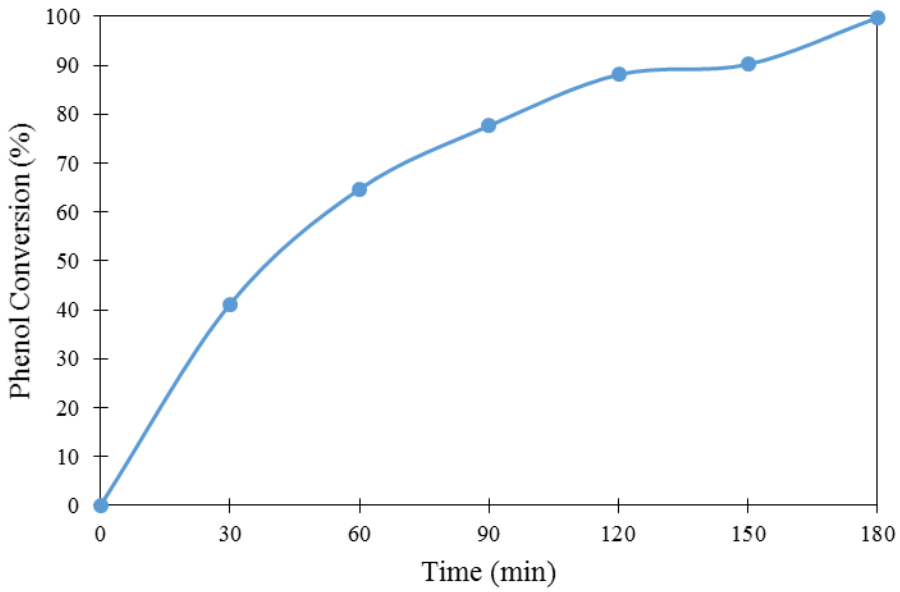

Figure 14: Phenol removal with time in a trickle bed reactor over Al/Zr-PILCs catalyst supported on a monolith (Experimental conditions: 160 °C, 10 bar, 0.012 m/s).

Generally, phenol is broken down to aromatics, carboxylic acid and CO_2 inside the reactor depending on the reaction pathway followed (Baloyi et al, 2018c). In this work, the amount of

CO_2 released was measured by an online GC connected to the reactor and the results were plotted in Figure 15. As shown in Figure 15 the amount of CO_2 released increases with time and a large peak appeared within 3 h and immediately a sharp decrease was observed afterward signaling complete conversion of the pollutant.

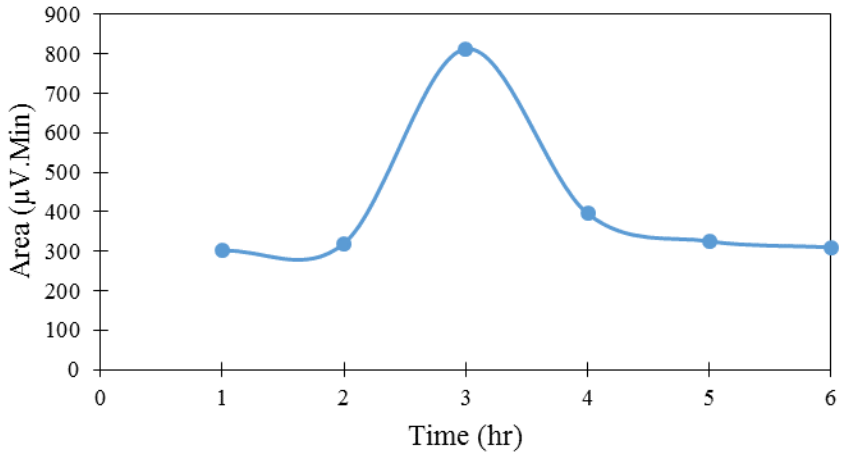

Figure 15: Amount of CO_2 released with time during phenol oxidation in CWAO process.

4.3 Influence of operating parameters

According to the preliminary investigation 10 bar was the optimum pressure and the results are not shown in this work. Figure 16 shows that at 120 °C and liquid flow rate of 10 mL/min the conversion of phenol is 86 %. Moreover, an increase in temperature to 140 °C or 160 °C while keeping liquid flow rate and pressure constant (10 mL/min, 10 bar) resulted in the high conversion of phenol 91 and 100%, respectively. This behavior can be attributed to the reaction rate constant which is a function of temperature and activation energy, according to the Arrhenius equation (22):

$$k = A.\exp(\frac{-E_a}{RT}) \quad (22)$$

where k is the reaction rate constant, A is a pre-exponential factor, E_a is activation energy, R is ideal gas constant and T is the temperature. Furthermore, an increase in temperature results in a decrease in liquid viscosity which facilitates the transfer of reactants from bulk liquid to the surface of the catalyst (Mohammed *et al.*, 2016). The same observations were reported by Abid et al, 2016 when activated carbon catalyst was used. They reported that 64, 87 and 97% of phenol was converted at 120, 140 and 160 °C. Similarly, Mohammed *et al.*, 2016 reported that 88% of phenol was converted at 120 °C and when the temperature was increased to 140 °C or

160 °C phenol conversion increased to 91 and 93%, respectively.

The effect of liquid flow rate on phenol conversion was also studied in the range (10, 20, 30 and 40 mL/min) while keeping other parameters constant (gas flow rate = 0.012 m/s and pressure = 10 bar). As shown in Figure 16 an increase in liquid flow rate has a negative impact on phenol conversion due to increase in liquid flow rate reduces residence time resulting in less contact time between the phases. Furthermore, the high liquid flow rate increases film thickness and liquid holdup which decreases contact time between gas and liquid on the catalyst active sites resulting in high resistance to mass transfer. When the reaction temperature was kept constant at 120 °C while varying liquid flow rate between (10, 20, 30 and 40 mL/min), phenol conversion decreased as follows 86, 79, 69 and 64%, respectively. Similarly, phenol conversion decreased from 91 to 70% when the liquid flow rate was increased from 10 to 40 mL/min while keeping the temperature constant at 140 °C. Moreover, when the temperature was increased to 160 °C while varying liquid flow rate between 10 and 40 mL/min phenol conversion also decreased from 100 to 85%. Abid et al., 2016 reported similar behaviour, phenol conversion was 79% at 1.662 mL/min, while the conversion increased to 87% and 96% at 0.996 and 0.6 mL/min.

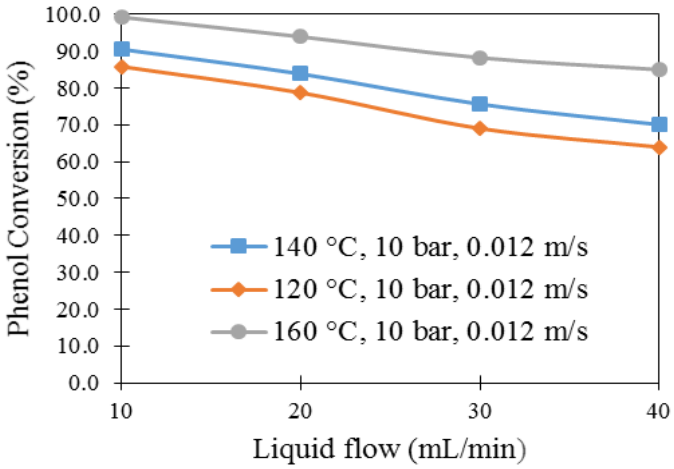

Figure 16: Phenol conversion with liquid flow rate and change in reaction temperature.

4.4 Kinetic model

The reaction kinetics is required to provide a complete interpretation of data obtained in a fixed

bed monolithic reactor operated in a trickle flow mode during phenol oxidation. When a simple power-law model was used to estimate kinetic parameters as in (Eftaxias *et al.*, 2005c; Abid et al, 2014a; Abid et al, 2016) equations 23 to 28 were employed.

$$-r_{ph} = k_{ob}.C_{ph}^{\alpha} \tag{23}$$

And k_{ob} can be expressed as follow,

$$K_{ob} = k_o.exp(\tfrac{-E_{ob}}{RT}).P_{O_2}^{\beta} \tag{24}$$

Since the reaction takes place in a liquid phase the above equation becomes,

$$K_{ob} = k_o.exp(\tfrac{-E_{ob}}{RT}).X_{O_2}^{\beta} \tag{25}$$

Assuming that the vapour phase behaves ideally (Eze & Masuku 2018), then the oxygen mole fraction (X_{O2}) was calculated using Henry's law (Mohammed 2014)

$$P_{O_2} = X_{O_2}.\mathrm{H} \tag{26}$$

Equation 25 can be linearized by taking logarithm on both sides of the equation,

$$InK_{ob} = Ink_o + \beta InX_{O_2} - (\tfrac{-E_{ob}}{RT}) \tag{27}$$

Where α and β are reaction order with respect to phenol and oxygen, E_{ob} is activation energy, H is Henry's constant while k_o is the pre-exponential factor. By assuming ideal plug flow and first order with respect to phenol, equation 25 was integrated and rearranged to obtain K_{ob} as follow,

$$k_{ob} = -(\tfrac{1}{\tau})In(1 - x_{ph}) \tag{28}$$

K_{ob} was applied to the experimental data by plotting the graph of $In(1-x_{ph})$ vs τ as shown in Figure 17 and a perfect fit was found at 160 °C with R^2 value equal to 0.9988 (Abid et al., 2014a; Abid et al., 2016). The activation energy was calculated from the slope of the line in Figure 18.

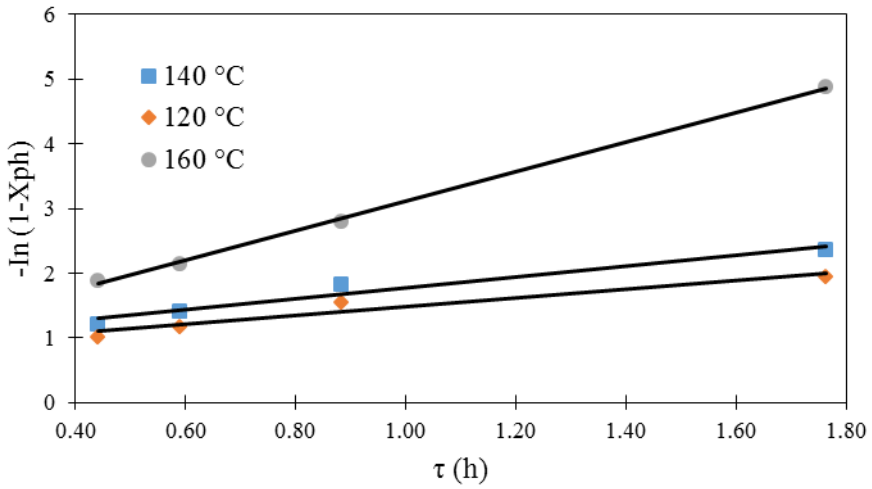

Figure 17: Graph of In(1-Xph) vs τ at 10 bar and temperatures ranging between 120, 140 and 160 °C.

$$Ink_{0b} = \frac{-5086.5}{T} + 12.425 \quad (29)$$

E_{ob} = 42.289 kJ/mol

A wide range of activation energies were reported in open literature as 21.306 kJ/mol (Moma et al; 2018), 85 kJ/mol (Fortuny et al., 1999), 29.299 kJ/mol (Abid et al., 2014a), 35.4 kJ/mol (Wu et al., 2005) and 74.9 kJ/mol (Eftaxias et al., 2001) using different catalysts and the results obtained in this study are within the range. These results provide a basis to develop a computational fluid dynamics model of this system which would be instrumental in identifying liquid mal-distribution and preventing the formation of hotspots (Kapfunde et al., 2018).

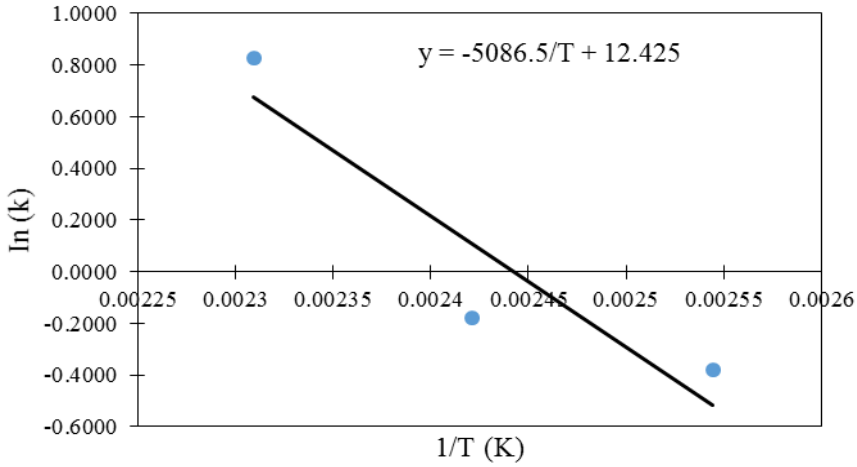

Figure 18: Plot of In(k) versus 1/T at a pressure of 10 bar and temperatures of 120, 140, and 160 °C.

4.5 Euler-Euler computational model

A mixture of phenol (C_6H_5OH) and oxygen (O_2) was fed to the isothermal-isobaric reactor operated at 160 °C and 10 bar. The gas and liquid inlet velocities were kept constant at 0.012 and 0.00007 m/s, respectively. As shown in Figure 19(a), the contours of phenol mass fraction indicate that the pollutant is highly concentrated in the top half of the reactor. However, the concentration is sharply decreased as the stream moves through the reactor and phenol is completely oxidized to form byproduct such as carbon dioxide (CO_2). In addition, Figure 19(b) shows a concentration profile of CO_2 inside the reactor and from these results, it can be concluded that C_6H_5OH was completely mineralized. These results are consistent with the findings of (Lopes & Quinta-Ferreira 2010), in their study phenolic acid was oxidized in a TBR and simulated using Euler-Euler method at 160 & 200 °C. They concluded that 82 % of total organic carbon (TOC) was converted at 160 °C whereas only 84.8 % was converted at 200 °C.

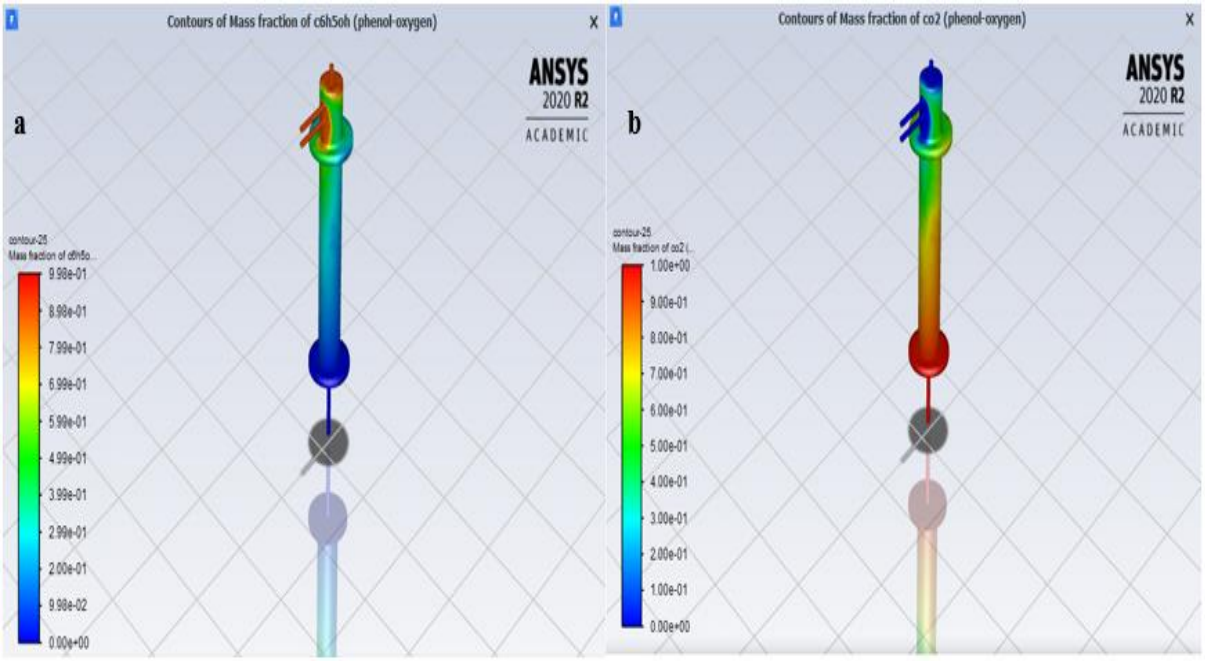

Figure 19: Contours of phenol mass fraction (a) and CO_2 profile inside the reactor (b).

Figure 20 shows that phenol is highly concentrated at the reactor wall and there is a sharp decrease in concentration when you move away from the wall towards the center of the reactor.

Furthermore, no phenol was detected at the center of the reactor and a flat distribution profile was observed. It can be concluded from these findings that there is no liquid at the center of the reactor due to channeling which might lead to the formation of a hot spot at the center.

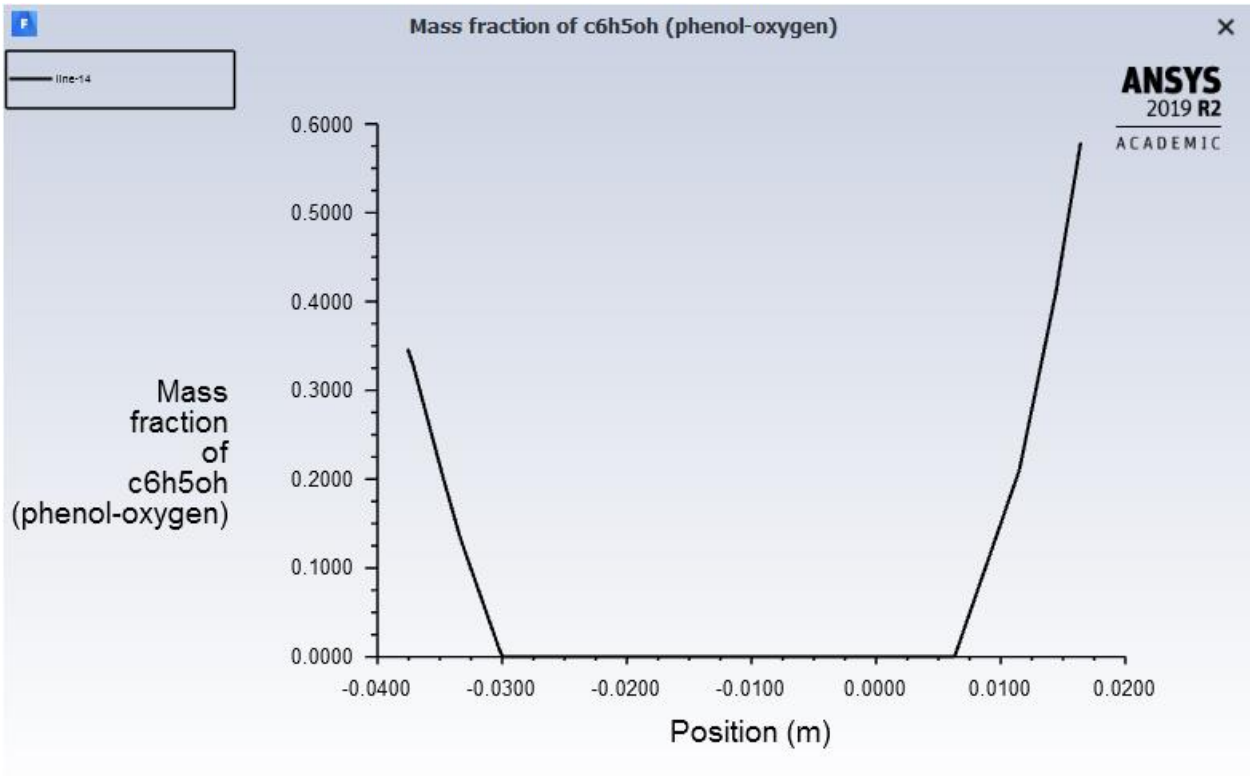

Figure 20: Phenol mass fraction distribution in a radial direction.

Phenolic wastewater is highly toxic and refractory to biological wastewater treatment method. The use of CWAO for treatment of phenolic wastewater is gaining interest due to advances in heterogeneous catalysis. Furthermore, the use of newly developed catalysts that are cheap, highly reactive, selective and hydrothermally stable makes the process more economic (Guo and Al-Dahhan, 2003; Baloyi et al., 2018c). In addition, phenol can be completely mineralized to CO_2 and water (H_2O) at mild operating conditions. This statement is supported by the results shown in Figure 21 when phenol was oxidized at 160 °C and 10 bar. From the observations, the concentration profile of phenol inside the reactor is close to zero along the reactor bed. These results are in agreement with the findings in our previous work (Makatsa et al, 2019).

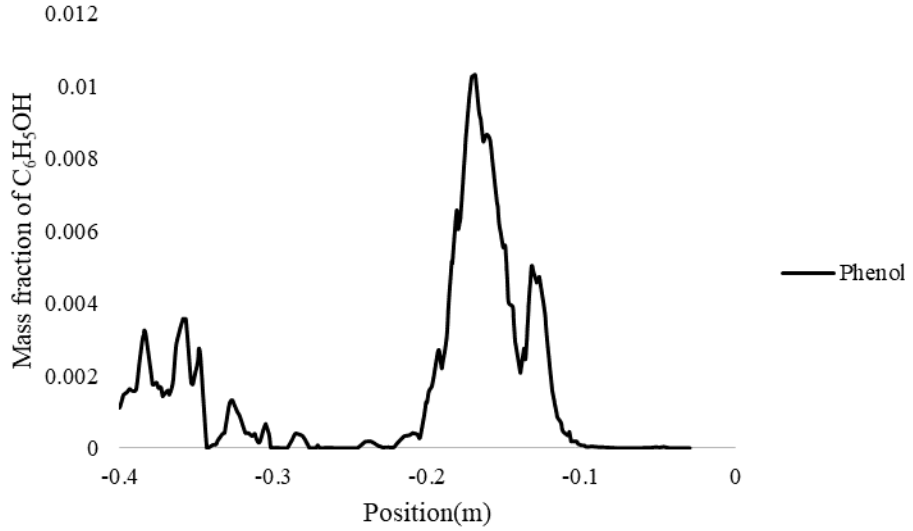

Figure 21: Mass fraction of phenol inside the reactor bed

Zhang et al, 2019 suggested that temperature distribution profile is affected by the packing structure and flow regime. Figure 22 shows a temperature distribution profile of phenol oxidation in a TBR when the reactor was operated in a trickle flow regime. The results indicate that the temperature profile is not symmetric suggesting that the packing structure is non-uniform. Moreover, a flat temperature profile is seen at the bottom of the reactor. However, a bulge is observed at the top half of the reactor indicating excess heat generated due to channeling of liquid. From these observations, it can be concluded that a hot spot is formed at the top section of the reactor bed.

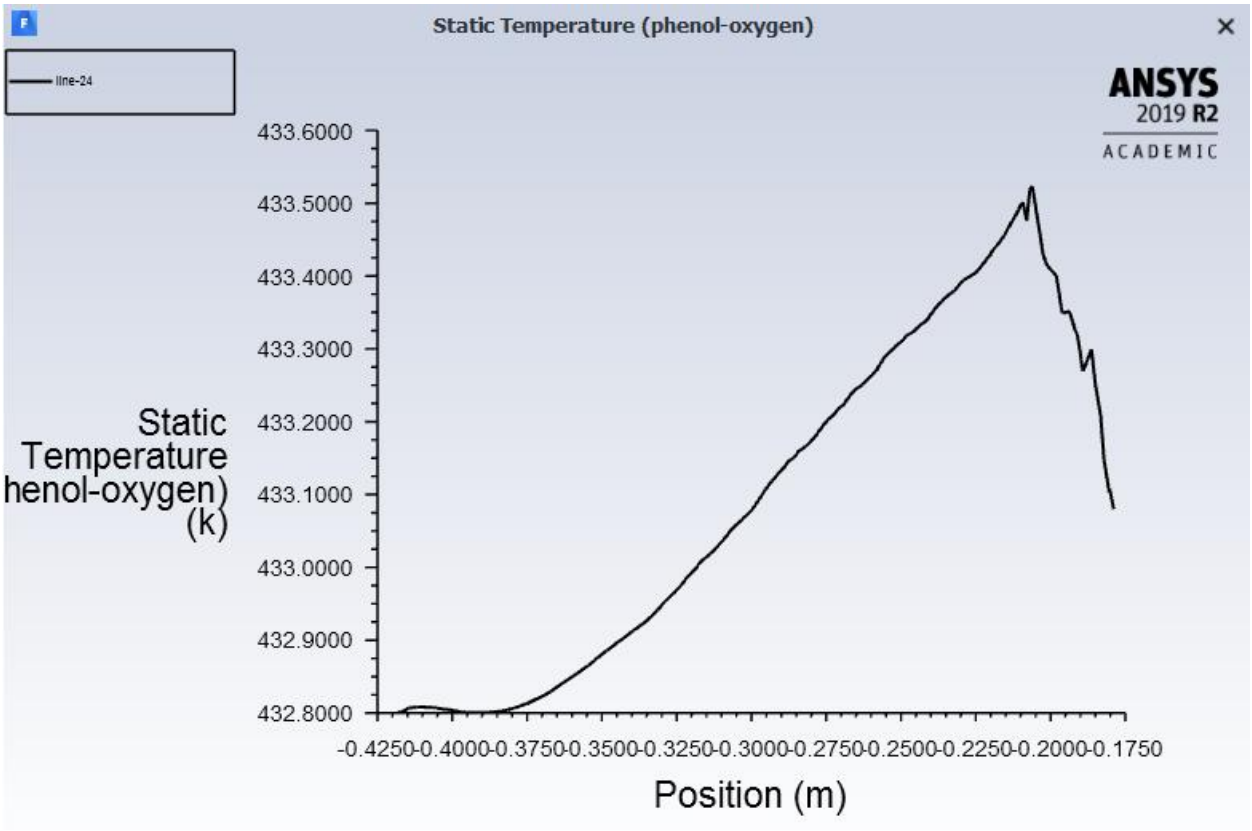

Figure 22: Temperature profile along the reactor bed at 160 °C.

Figure 23 represents the radial temperature distribution profile inside the reactor. The results show that wall temperature is constant. However, excess heat is generated when you start to move away from the wall indicating the formation of a hot spot. Furthermore, there is a temperature difference of 2.5 K between the hot spot and the surrounding area due to channeling effect (Wehinger et al., 2019). These results are comparable to the findings of Lopes and Quinta-Ferreira, (2010). In their study, phenol oxidation was simulated in a TBR at 160 and 200 °C using the Eulerian model. The authors reported a temperature difference of 0.2 °C and 3.7 °C between the center and reactor wall.

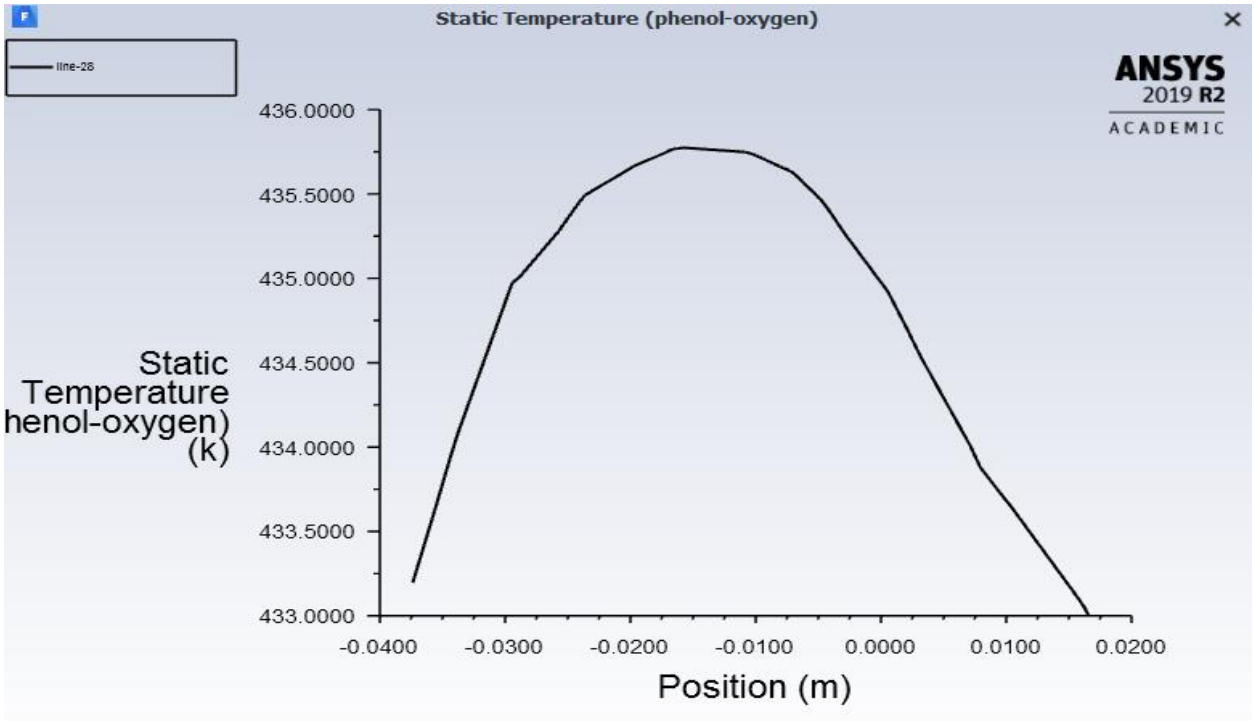

Figure 23: Radial temperature profile inside the reactor at 160 °C.

The main disadvantage of TBR is high-pressure drop resulting in energy losses and thus, making the process expensive. However, this problem can be solved by incorporating the monolith into the reactor packing. Several researchers have investigated the effect of packing structures on pressure drop using different packing materials and concluded that monolith has a lower pressure drop (Guo et al., 2018; Manoharan and Buwa, 2019). This phenomenon is clearly seen in Figure 24; the results indicate that there is an increased in pressure at 0.22 m (monolith 1) and 0.25 m (monolith 2). In their study Manoharan and Buwa, (2019) attributed the increase in pressure inside the monolith channels to low-velocity profile leading to low backflow.

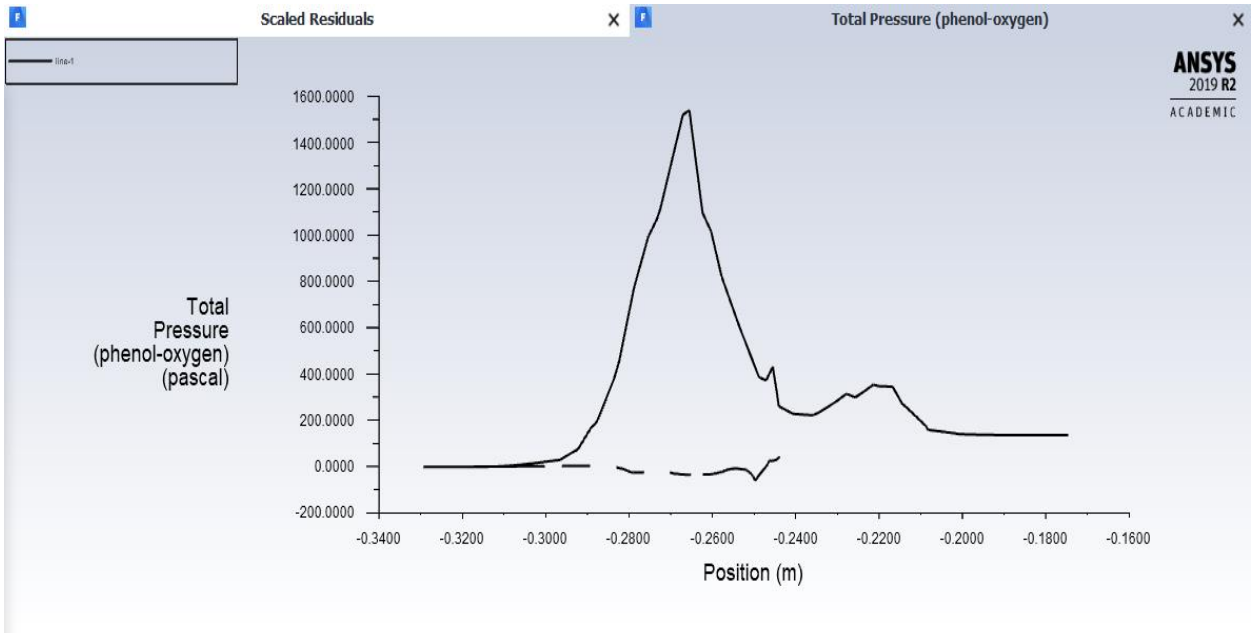

Figure 24: Axial pressure distribution profile inside the reactor.

Chapter 5: Conclusions and Recommendations

5.1 Conclusions

Bentonite clay was successfully pillared with metal oxides of alumina and zirconia. This is confirmed by an increased surface area and a shift of montmorillonite peak from high to low angle. After wash coating, the catalyst on the surface of the monolith, bentonite peaks disappeared indicating the formation of amorphous SiO_2. It can be concluded from SEM analysis that no cracks are formed on the surface of the monolith and this can be attributed to the use of glycerol. A sample dried using thermally assisted microwave oven is smoother compared to others. This is due to heat that is homogeneously dispersed in the microwave.

Phenol oxidation was studied in a fixed bed monolithic reactor operated in a trickle flow mode over Al/Zr pillared clay catalyst. The rate of phenol degradation was improved by an increase in temperature whereas an increase in liquid flow rate showed an opposite trend. The complete conversion was reached after 3 h. A simple power law model was used to determine activation energy from a linear plot and found to be 42.289 kJ/mol.

After catalyst activity was tested in a TBR, CFD model (Euler-Euler) was developed from the kinetics of the process. The reactor model was simulated at 160 °C, 10 bar and CFD results showed that phenol was completely removed leaving significant amount of CO_2. However, temperature profile indicated that there is a hot spot near the center of the reactor which might lead to catalyst deactivation. Furthermore, axial pressure profile showed that incorporating the monolith in the packing structure helped to minimize pressure losses.

5.2 Potential for industrialization

For years industrialization of pillared clay catalyst has been hindered by prolonged synthesis time (1-5 days) and a large amount of water used. Until recently, PILCs have been limited to laboratory applications as there is great difficulty in shaping them from powders to commercial shapes. However, recent studies indicated that the time taken to synthesize the catalyst can be reduced significantly by ultra-sonication and direct addition of powder bentonite clay to the pillaring solution. Furthermore, the catalyst can be easily scaled-up by wash coating the catalyst on the surface of cordierite monolith support because the conditions inside the monolith channels

remain the same irrespective of size. The only challenges associated with industrialization of this process will be, a large amount of wastewater generated in the washing process and ultra-sonicating of an increased amount of catalyst slurry. A downstream process should be developed to treat and recycle wastewater generated in the washing process because this will increase the economics of the process.

5.3 Recommendations

1. The reactor must be fitted with liquid distributer
2. It is recommended that hydrodynamics of the process be investigated experimentally and the results must be validated using CFD model.
3. The reactor bed must be fitted with at least three temperature probes to monitor bed temperature.
4. The reactor must be fitted with differential pressure transducer to record pressure drop.
5. When the catalyst is commercialized a lot of wastewater will be generated from the washing process and this waste should be treated before discharging it.

Reference

Abbas, ZI & Abbas, AS. 2019. Oxidative degradation of phenolic wastewater by electro-fenton process using MnO_2 -graphite electrode. *Journal of Environmental Chemical Engineering*. 7(3):103108. doi.org/10.1016/j.jece.2019.103108.

Abid, MF, Jasim, FT & Ahmed, LS. 2014. Kinetic study of phenol removal from wastewater over a 0.5% Pt / γ -Al_2O_3 catalyst in a trickle bed reactor. 13(5):2014.

Abid, MF, Alwan, GM & Abdul-Ridha, LA. 2016. Study on Catalytic Wet Air Oxidation Process for Phenol Degradation in Synthetic Wastewater Using Trickle Bed Reactor. *Arabian Journal for Science and Engineering*. 41(7):2659–2670. doi.org/10.1007/s13369-016-2171-x.

Adamowska, MB & Costa, P Da. 2014. Structured Pd / γ-Al_2O_3 Prepared by Washcoated Deposition on a Ceramic Honeycomb for Compressed Natural Gas Applications. *Journal of Nanoparticles*. 2015:10–12. doi.org/http://dx.doi.org/10.1155/2015/601941.

Adekola, O & Majozi, T. 2017. Wastewater minimization in batch plants with sequence dependent changeover. *Computers & Chemical Engineering*. 97:85–103. doi.org/https://doi.org/10.1016/j.compchemeng.2016.11.016.

Ahmed, LS. 2012. Hydrodynamics and Kinetics Study of Phenol Removal Treatment in wastewater in a Trickle Bed Reactor. *Thesis*.

Al-obaidi, MA, Kara-zaïtri, C & Mujtaba, IM. 2019a. Performance evaluation of multi-stage reverse osmosis process with permeate and retentate recycling strategy for the removal of chlorophenol from wastewater. *Computers and Chemical Engineering*. 121:12–26. doi.org/10.1016/j.compchemeng.2018.08.035.

Al-obaidi, MA, Kara-zaïtri, C & Mujtaba, IM. 2019b. Evaluation of chlorophenol removal from wastewater using multi-stage spiral-wound reverse osmosis process via simulation. *Computers and Chemical Engineering*. 130:106522. doi.org/10.1016/j.compchemeng.2019.106522.

Al-Obaidi, MA, Kara-Zaïtri, C & Mujtaba, IM. 2017. Removal of phenol from wastewater using spiral-wound reverse osmosis process: Model development based on experiment and simulation. *Journal of Water Process Engineering*. 18:20–28. doi.org/https://doi.org/10.1016/j.jwpe.2017.05.005.

Alves, APA, Lima, PS, Dezotti, M & Bassin, JP. 2017. Impact of phenol shock loads on the performance of a combined activated sludge-moving bed bio film reactor system. *International Biodeterioration & Biodegradation*. 123:146–155. doi.org/10.1016/j.ibiod.2017.06.015.

Arena, F, Italiano, C, Raneri, A & Saja, C. 2010. Mechanistic and kinetic insights into the wet air oxidation of phenol with oxygen (CWAO) by homogeneous and heterogeneous transition-metal catalysts. *Applied Catalysis B: Environmental*. 99(1–2):321–328. doi.org/10.1016/j.apcatb.2010.06.039.

Arena, F, Italiano, C & Spadaro, L. 2012. Applied Catalysis B : Environmental Efficiency and reactivity pattern of ceria-based noble metal and transition metal-oxide catalysts in the wet air oxidation of phenol. *"Applied Catalysis B, Environmental"*. 115–116:336–345. doi.org/10.1016/j.apcatb.2011.12.035.

Attou, A & Ferschneider, G. 1999. A two fluid model for flow regime transition in gas liquid trickle-bed reactors. 54:5031–5037.

Baloyi, SJ. 2019. Pillared clays as " green chemistry '' catalysts for wastewater treatment. Witwatersrand.

Baloyi, J, Ntho, T & Moma, J. 2018a. Synthesis and application of pillared clay heterogeneous catalysts for wastewater treatment: a review. *RSC Advances*. doi.org/10.1039/C7RA12924F.

Baloyi, J, Ntho, T & Moma, J. 2018b. Synthesis of highly active and stable Al/Zr pillared clay as

catalyst for catalytic wet oxidation of phenol. *Journal of Porous Materials*. (August). doi.org/10.1007/s10934-018-0667-3.

Baloyi, J, Ntho, T & Moma, J. 2018c. A Novel Synthesis Method of Al/Cr Pillared Clay and its Application in the Catalytic Wet Air Oxidation of Phenol. *Catalysis Letters*. 0(0):0. doi.org/10.1007/s10562-018-2579-x.

Beni, AH & Khosravi-Nikou, MR. 2015. Modeling Hydrodynamics of Trickle-bed Reactors at High and Low Pressure Using CFD Method. *Petroleum Science and Technology*. 33(20):1770–1779. doi.org/10.1080/10916466.2011.588639.

Braga, A, Ribeiro, M, Noronha, FB, Maria, J, Bueno, C & Santos, JB. 2018. The effects of Co addition to supported Ni catalysts on hydrogen production from oxidative steam reforming of ethanol. *Energy and Fuels*. 32:12814–12825. doi.org/10.1021/acs.energyfuels.8b02727.

Cao, Y, Li, B, Zhong, G, Li, Y, Wang, H, Yu, H & Peng, F. 2018. Catalytic wet air oxidation of phenol over carbon nanotubes: Synergistic effect of carboxyl groups and edge carbons. *Carbon*. 133:464–473. doi.org/10.1016/j.carbon.2018.03.045.

Castaldo, R, Iuliano, M, Cocca, M, Ambrogi, V, Gentile, G & Sarno, M. 2019. A New Route for Low Pressure and Temperature CWAO: A PtRu/MoS_2_Hyper-Crosslinked Nanocomposite. *Nanomaterials*. 9(10):1477. doi.org/10.3390/nano9101477.

Cecilia Sánchez-Trinidad, Gloria del Angel, GT-T, Adrián Cervantes-Uribe, A. Abiu Silahua Pavón, ZG-Q & Juan Carlos Arévalo-Pérez, and FJT-M. 2019. *Effect of the $CuAl_2O_4$ and $CuAlO_2$ Phases in Catalytic Wet Air Oxidation of ETBE and TAME using CuO/γ-Al_2O_3 catalysts*. Available from: https://onlinelibrary.wiley.com/doi/pdf/10.1002/open.201900080 [Accessed 15 January 2020].

Chicinaş, RP, Gál, E, Bedelean, H, Darabantu, M & Măicăneanu, A. 2018. Novel metal modified diatomite, zeolite and carbon xerogel catalysts for mild conditions wet air oxidation of phenol: Characterization, efficiency and reaction pathway. *Separation and Purification Technology*. 197:36–46. doi.org/https://doi.org/10.1016/j.seppur.2017.12.050.

Crini, G & Lichtfouse, E. 2019. Advantages and disadvantages of techniques used for wastewater treatment. *Environmental Chemistry Letters*. 17(1):145–155. doi.org/10.1007/s10311-018-0785-9.

Cybulski, A. 2007. Catalytic wet air oxidation: Are monolithic catalysts and reactors feasible? *Industrial and Engineering Chemistry Research*. doi.org/10.1021/ie060906z.

Davies, D, Golunski, S, Johnston, P, Lalev, G & Taylor, SH. 2018. Dominant effect of support wettability on the reaction pathway for catalytic wet air oxidation over Pt and Ru nanoparticle catalysts. *ACS Catalysis*. 8(4):2730–2734. doi.org/10.1021/acscatal.7b04039.

Dewidar, H, Nosier, SA & El-Shazly, AH. 2018. Photocatalytic degradation of phenol solution using Zinc Oxide/UV. *Journal of Chemical Health and Safety*. 25(1):2–11. doi.org/10.1016/j.jchas.2017.06.001.

Eftaxias, A. 2002a. Catalytic wet air oxidation of phenol in a trickle bed reactor: Kinetics and reactor modelling. Thesis.

Eftaxias, A. 2002b. Catalytic Wet Air Oxidation of Phenol in a Trickle Bed Reactor: Kinetics and Reactor Modelling. (December):196.

Eftaxias, A, Font, J, Fortuny, A, Giralt, J, Fabregat, A & Stuber, F. 2001. Kinetic modelling of catalytic wet air oxidation of phenol by simulated annealing. *Applied Catalysis B-Environmental*. 33(2):175–190.

Eftaxias, A, Font, J, Fortuny, A, Fabregat, A & Uber, FS. 2005. Kinetics of phenol oxidation in a trickle bed reactor over active carbon catalyst. *Journal of Chemical Technology and Biotechnology J Chem Technol Biotechnol*. 80:677–687. doi.org/10.1002/jctb.1250.

Eftaxias, A, Font, J, Fortuny, A, Fabregat, A & Stüber, F. 2005. Kinetics of phenol oxidation in a trickle bed reactor over active carbon catalyst. *Journal of Chemical Technology and Biotechnology*. doi.org/10.1002/jctb.1250.

Eftaxias, A, Font, J, Fortuny, A, Fabregat, A & Stu, F. 2006. Catalytic wet air oxidation of phenol over active carbon catalyst Global kinetic modelling using simulated annealing. 67:12–23. doi.org/10.1016/j.apcatb.2006.04.012.

El-Ashtoukhy, ESZ, El-Taweel, YA, Abdelwahab, O & Nassef, EM. 2013. Treatment of petrochemical wastewater containing phenolic compounds by electrocoagulation using a fixed bed electrochemical reactor. *International Journal of Electrochemical Science*. 8(1):1534–1550.

Elmer, TH. 2008. Selective leaching of extruded cordierite honeycomb structures. In: *Applications of Refractories: Ceramic Engineering and Science Proceedings*. W. Smothers, Ed. John Wiley & Sons, Ltd. 40–51. doi.org/10.1002/9780470320310.ch4.

Eze, PC & Masuku, CM. 2018. Vapour–liquid equilibrium prediction for synthesis gas conversion using artificial neural networks. *South African Journal of Chemical Engineering*. 26:80–85. doi.org/https://doi.org/10.1016/j.sajce.2018.10.001.

Fortuny, A, Ferrer, C, Bengoa, C, Font, J & Fabregat, A. 1995. Catalytic removal of phenol from aqueous-phase using oxygen or air as oxidant. *Catalysis Today*. 24(1–2):79–83.

Fortuny, A, Bengoa, C, Font, J, Castells, F & Fabregat, A. 1999. Water pollution abatement by catalytic wet air oxidation in a trickle bed reactor. *Catalysis Today*. 53:107–114. Available from: http://www.etseq.urv.cat/CREPI/webc/publipdf/027.pdf [Accessed 24 May 2018].

Frascari, D, Rubertelli, G, Arous, F, Ragini, A, Bresciani, L, Arzu, A & Pinelli, D. 2019. Valorisation of olive mill wastewater by phenolic compounds adsorption : Development and application of a procedure for adsorbent selection. *Chemical Engineering Journal*. 360(September 2018):124–138. doi.org/10.1016/j.cej.2018.11.188.

Gao, P, Song, Y, Wang, S, Descorme, C & Yang, S. 2018. Fe_2O_3 -CeO_2 -Bi_2O_3 /γ-Al_2O_3 catalyst in the catalytic wet air oxidation (CWAO) of cationic red GTL under mild reaction conditions. *Frontiers of Environmental Science and Engineering*. 12(1). doi.org/10.1007/s11783-018-1025-z.

Garg, A & Mishra, A. 2013. Degradation of organic pollutants by wet air oxidation using nonnoble metal-based catalysts. *Journal of Hazardous, Toxic, and Radioactive Waste*. 17(2):89–96. doi.org/10.1061/(ASCE)HZ.2153-5515.0000152.

Guerra-que, Z, Hermicenda, P, Abiu, A, Pav, S, Monteros, AEDL & Lunag, MA. 2019. Treatment of phenol by catalytic wet air oxidation: A comparative study of copper and nickel supported on γ-alumina, ceria and γ-alumina–ceria. *Royal Society of Chemistry*. 9:8463–8479. doi.org/10.1039/c9ra00509a.

Guo, J & Al-Dahhan, M. 2003. Kinetics of Wet Air Oxidation of Phenol over a Novel Catalyst. *Industrial & Engineering Chemistry Research*. 42(22):5473–5481. doi.org/10.1021/ie0302488.

Guo, Y, Dai, C & Lei, Z. 2018. Hydrodynamics and mass transfer in multiphase monolithic reactors with different distributors: An experimental and modeling study. *Chemical Engineering and Processing: Process Intensification*. 125(February):234–245. doi.org/10.1016/j.cep.2018.01.026.

Hamoudi, S.; Larachi, F.;Graciela, C.;Myrian, C. 1998. Wet oxidation of phenol catalyzed by unpromoted and platinum promoted manganese/cerium oxide. *Industrial & Engineering Chemistry Fundamentals*. 37:3561.

Haro, P, Johnsson, F & Thunman, H. 2016. Improved syngas processing for enhanced Bio-SNG production: A techno-economic assessment. *Energy*. 101:380–389.

doi.org/https://doi.org/10.1016/j.energy.2016.02.037.

John Moma; Thabang Ntho; Siwela Jeffrey Baloyi. 2018. Influence of operational parameters and kinetic modelling of catalytic wet air oxidation of phenol by Al/Zr pillared clay catalyst. *Iranian Journal of chemistry and chemical engineering*. 37.

Kapfunde, N, Masuku, CM & Hildebrandt, D. 2018. Optimization of the Thermal Efficiency of a Fixed-Bed Gasifier using Computational Fluid Dynamics. In: *13th International Symposium on Process Systems Engineering (PSE 2018)*. V. 44. M.R. Eden, M.G. Ierapetritou, & G.P. Towler, Eds. (Computer Aided Chemical Engineering). Elsevier. 1747–1752. doi.org/https://doi.org/10.1016/B978-0-444-64241-7.50286-X.

Klinghoffer, AA, Cerro, RL & Abraham, MA. 1998. Catalytic wet oxidation of acetic acid using platinum on alumina monolith catalyst. 40:59–71.

Krastanov, A, Alexieva, Z & Yemendzhiev, H. 2013. Microbial degradation of phenol and phenolic derivatives. 76–87. doi.org/10.1002/elsc.201100227.

Kuzeljevic, Z. 2010. Hydrodynamics Of Trickle Bed Reactors: Measurements And Modeling. Available from: http://openscholarship.wustl.edu/etd.

Lai, C, He, T, Li, X, Chen, F, Yue, L & Hou, Z. 2019. Catalytic wet air oxidation of phenols over porous plate Cu-based catalysts. *Applied Clay Science*. 181:105253. doi.org/https://doi.org/10.1016/j.clay.2019.105253.

Lal, K & Garg, A. 2014. Catalytic wet oxidation of phenol under mild operating conditions : development of reaction pathway and sludge characterization. (January 2015). doi.org/10.1007/s10098-014-0777-9.

Lal, K & Garg, A. 2016. Catalytic wet oxidation of phenol under mild operating conditions : development of reaction pathway and sludge characterization. (January 2015). doi.org/10.1007/s10098-014-0777-9.

Levec, J. 1995. Catalytic oxidation of aqueous solutions of organics. An effective method for removal of toxic pollutants from waste waters. 24:51–58.

Liu, C, Min, Y, Zhang, A, Si, Y, Chen, J & Yu, H. 2019. Electrochemical treatment of phenol-containing wastewater by facet- tailored TiO_2 : Efficiency , characteristics and mechanisms. *Water Research*. 165:114980. doi.org/10.1016/j.watres.2019.114980.

Lopes, RJG & Quinta-Ferreira, RM. 2007. Trickle-bed CFD studies in the catalytic wet oxidation of phenolic acids. *Chemical Engineering Science*. 62(24):7045–7052.

doi.org/10.1016/j.ces.2007.08.085.

Lopes, RJG & Quinta-Ferreira, RM. 2010. Assessment of CFD Euler-Euler method for trickle-bed reactor modelling in the catalytic wet oxidation of phenolic wastewaters. *Chemical Engineering Journal*. 160(1):293–301. doi.org/10.1016/j.cej.2010.03.024.

de los Monteros, AE, Lafaye, G, Cervantes, A, Angel, G Del, Jr., JB & Torres, G. 2015. Catalytic wet air oxidation of phenol over metal catalyst (Ru,Pt) supported on TiO_2–CeO_2 oxides. *Catalysis Today*. 258:564–569. doi.org/https://doi.org/10.1016/j.cattod.2015.01.009.

Luo, Z, Gao, M, Yang, S & Yang, Q. 2015. Adsorption of phenols on reduced-charge montmorillonites modified by bispyridinium dibromides: Mechanism, kinetics and thermodynamics studies. *Colloids and Surfaces A: Physicochemical and Engineering Aspects*. 482:222–230. doi.org/10.1016/J.COLSURFA.2015.05.014.

Makatsa, TJ, Baloyi, SJ, Ntho, TA & Masuku, CM. 2019. Kinetic study of phenol oxidation in a trickle bed reactor over Al/Zr-pillared clay catalyst. *IOP Conference Series: Materials Science and Engineering*. 655:12050. doi.org/10.1088/1757-899x/655/1/012050.

Makatsa, TJ, Baloyi, J, Ntho, T & Masuku, CM. 2020. Catalytic wet air oxidation of phenol: Review of the reaction mechanism, kinetics, and CFD modeling. *Critical Reviews in Environmental Science and Technology*. (June, 11):1–33. doi.org/10.1080/10643389.2020.1771886.

Manoharan, KG & Buwa, VV. 2019. Structure-resolved CFD simulations of different catalytic structures in a packed bed. *Industrial & Engineering Chemistry Research*. 58(49):22363–22375. doi.org/10.1021/acs.iecr.9b03537.

Martin Zhuwakinyu and the Research Unit of Creamer media. 2018. A review of South Africa ' s water sector. *Research channel africa*. (November).

Masuku, CM & Biegler, LT. 2019. Recent advances in gas-to-liquids process intensification with emphasis on reactive distillation. *Current Opinion in Chemical Engineering*. doi.org/https://doi.org/10.1016/j.coche.2018.12.009.

Maugans, CB & Akgerman, A. 2003. Catalytic wet oxidation of phenol in a trickle bed reactor over a Pt/TiO2 catalyst. *Water Research*. 37(2):319–328. doi.org/10.1016/S0043-1354(02)00289-0.

Minhua, Z, He, D & Zhongfeng, G. 2019. A particle-resolved CFD model coupling reaction-diffusion inside fixed-bed reactor. *Advanced Powder Technology*. 30(6):1226–1238.

doi.org/10.1016/j.apt.2019.03.019.

Moghaddam, EM, Foumeny, EA, Stankiewicz, AI & Padding, JT. 2019. Fixed bed reactors of non-spherical pellets: Importance of heterogeneities and inadequacy of azimuthal averaging. *Chemical Engineering Science: X*. 1:100006. doi.org/https://doi.org/10.1016/j.cesx.2019.100006.

Mohammad F.Abid, FTJ & S.Ahmed, L. 2014. Kinetic study of phenol removal from wastewater over a 0.5% Pt/γ-Al_2O_3 catalyst in a trickle bed reactor. *Environmental Engineering and Management*. 13:1265–1275.

Mohammed, WT. 2014. Active Carbon from Date Stones for Phenol Oxidation in Trickle Bed Reactor, Experimental and Kinetic Study. 20(4):120–160.

Mohammed, WT & Abdullah, SM. 2008. Kinetic Study on Catalytic Wet Air Oxidation of Phenol in a Trickle Bed. 9(2).

Mohammed, AE, Jarullah, AT, Gheni, SA & Mujtaba, IM. 2016a. Optimal design and operation of an industrial three phase reactor for the oxidation of phenol. *Computers and Chemical Engineering*. 94:257–271. doi.org/10.1016/j.compchemeng.2016.07.018.

Mohino, F, Martin, AB, Salerno, P, Bahamonde, A & Mendioroz, S. 2005. High surface area monoliths based on pillared clay materials as carriers for catalytic processes. 29:125–136. doi.org/10.1016/j.clay.2004.12.003.

Moma, J, Baloyi, J & Ntho, T. 2018. Synthesis and characterization of an efficient and stable Al/Fe pillared clay catalyst for the catalytic wet air oxidation of phenol †. doi.org/10.1039/c8ra05825c.

Monteros, AEDL, Lafaye, G, Cervantes, A, Del Angel, G, Barbier, J & Torres, G. 2015. Catalytic wet air oxidation of phenol over metal catalyst (Ru,Pt) supported on TiO_2-CeO_2oxides. *Catalysis Today*. doi.org/10.1016/j.cattod.2015.01.009.

Mousazadeh, F. 2013. Hot spot formation in trickle bed reactors. Thesis.

Pagliaro, BM, Rossi, M & Pagliaro, M. 2008. Glycerol : Properties and Production. 1–18.

Parvas, M, Haghighi, M & Allahyari, S. 2014. Degradation of phenol via wet-air oxidation over CuO/CeO_2-ZrO_2 nanocatalyst synthesized employing ultrasound energy: Physicochemical characterization and catalytic performance. *Environmental Technology (United Kingdom)*. 35(9):1140–1149. doi.org/10.1080/09593330.2013.863952.

Pervov, A & Nguyen, XQ. 2019. Application of reverse osmosis and nanofiltration techniques at municipal drinking water facilities. *E3S Web of Conferences*. 97.

Pradeep, N V, Anupama, S, Navya, K, Shalini, HN, Idris, M & Hampannavar, US. 2015. Biological removal of phenol from wastewaters : a mini review. 105–112. doi.org/10.1007/s13201-014-0176-8.

Quintanilla, A, Casas, JA & Mohedano, AF. 2006. Reaction pathway of the catalytic wet air oxidation of phenol with a Fe / activated carbon catalyst. 67:206–216. doi.org/10.1016/j.apcatb.2006.05.003.

Radwan, M, Gar Alalm, M & Eletriby, H. 2018. Optimization and modeling of electro-Fenton process for treatment of phenolic wastewater using nickel and sacrificial stainless steel anodes. *Journal of Water Process Engineering*. 22(January):155–162. doi.org/10.1016/j.jwpe.2018.02.003.

Resende, KA, Teles, CA, Jacobs, G, Davis, BH, Cronauer, DC, Kropf, AJ, Marshall, CL, Hori, CE, et al. 2018. Hydrodeoxygenation of phenol over zirconia supported Pd bimetallic catalysts. The effect of second metal on catalyst performance. *Applied Catalysis B: Environmental*. 232:213–231. doi.org/https://doi.org/10.1016/j.apcatb.2018.03.041.

Resini, C, Catania, F, Berardinelli, S, Paladino, O & Busca, G. 2008. Catalytic wet oxidation of phenol over lanthanum strontium manganite. *Applied Catalysis B: Environmental*. 84(3–4):678–683. doi.org/10.1016/j.apcatb.2008.06.005.

Santos, A, Yustos, P, Quintanilla, A, Rodr, S & Garc, F. 2002. Route of the catalytic oxidation of phenol in aqueous phase. 39:97–113.

Seadira, T, Gullapelli, S, Abraham, NT, Xiaojun, L, M, MC & Mike, S. 2018. doi.org/10.1515/revce-2016-0064.

Serra-Pérez, E, Álvarez-Torrellas, S, Águeda, VI, Delgado, JA, Ovejero, G & García, J. 2019. Insights into the removal of Bisphenol A by catalytic wet air oxidation upon carbon nanospheres-based catalysts: Key operating parameters, degradation intermediates and reaction pathway. *Applied Surface Science*. 473:726–737. doi.org/https://doi.org/10.1016/j.apsusc.2018.12.205.

Soghrati, E, Kazemeini, M, Rashidi, AM & Jafari, K. 2014. Development of a structured monolithic support with a CNT washcoat for the naphtha HDS process. *Journal of Thaiwan Institute of Chemical Engineers*. (May). doi.org/10.1016/j.jtice.2013.08.009.

Suárez-Ojeda, ME, Fabregat, A, Stüber, F, Fortuny, A, Carrera, J & Font, J. 2007. Catalytic wet air oxidation of substituted phenols: Temperature and pressure effect on the pollutant removal, the catalyst preservation and the biodegradability enhancement. *Chemical Engineering Journal*.

132(1–3):105–115. doi.org/10.1016/j.cej.2007.01.025.

Sun, J, Liu, X, Zhang, F, Zhou, J, Wu, J & Alsaedi, A. 2019. Insight into the mechanism of adsorption of phenol and resorcinol on activated carbons with different oxidation degrees. *Colloids and Surfaces A*. 563(October 2018):22–30. doi.org/10.1016/j.colsurfa.2018.11.042.

Sun, X, Wang, C, Li, Y, Wang, W & Wei, J. 2015. Treatment of phenolic wastewater by combined UF and NF/RO processes. *Desalination*. 355:68–74. doi.org/https://doi.org/10.1016/j.desal.2014.10.018.

Tałałaj, IA & Biedka Paweł and Bartkowska, I. 2019. Treatment of landfill leachates with biological pretreatments and reverse osmosis. *Environmental Chemistry Letters*. 17(3):1177–1193. doi.org/10.1007/s10311-019-00860-6.

Ukonu, PN. 2018. Heterogeneous catalytic wet air oxidation of industrial wastewater pollutant for environmental sustainability. University of Massachusetts Lowell.

United Nations Department of Economic and Social Affairs). 2017. *World Population Prospects The 2017 Revision: Key Findings and Advance Tables.*

United Nations World Water Assessment Programme. 2018. *The United Nations World Water Development Report 2018: Nature-Based Solutions for Water.*

Villegas, L, Masset, F & Guilhaume, N. 2007. Wet impregnation of alumina-washcoated monoliths : Effect of the drying procedure on Ni distribution and on autothermal reforming activity. 320:43–55. doi.org/10.1016/j.apcata.2006.12.011.

Villegas, L, Mashhadi, N, Chen, M, Mukherjee, D, Taylor, K & Biswas, N. 2016. A Short Review of Techniques for Phenol Removal from Wastewater. *Current Pollution Reports*. 2. doi.org/10.1007/s40726-016-0035-3.

Vivek V. Ranade, RVC & Gunjal, PR. 2011. *Trickle bed reactors*.

Wang, C, Xu, J, Yang, Z, Zhang, Z & Cai, Z. 2019. A field study of polychlorinated dibenzo-p-dioxins and dibenzofurans formation mechanism in a hazardous waste incinerator : Emission reduction strategies. *Journal of Cleaner Production*. 232:1018–1027. doi.org/10.1016/j.jclepro.2019.06.020.

Wang, J, Fu, W, He, X, Yang, S & Zhu, W. 2014. Catalytic wet air oxidation of phenol with functionalized carbon materials as catalysts: Reaction mechanism and pathway. *Journal of Environmental Sciences (China)*. 26(8):1741–1749. doi.org/10.1016/j.jes.2014.06.015.

Wehinger, GD, Kolaczkowski, ST, Schmalhorst, L, Beton, D & Torkuhl, L. 2019. Modeling fi

xed-bed reactors from metal-foam pellets with detailed CFD. *Chemical Engineering Journal*. 373(April):709–719. doi.org/10.1016/j.cej.2019.05.067.

Wu, Qiang, Xijun Hu, PL. 2005. Kinetics Study on Heterogeneous Catalytic Wet Air Oxidation of Phenol using Copper / Activated CarbonCatalyst Kinetics Study on Heterogeneous Catalytic Wet Air Oxidation of Phenol using Copper / Activated Carbon Catalyst. *International Journal of Chemical Reactor Engineering*. 3.

Yadav, A, Teja, AK & Verma, N. 2016. Removal of phenol from water by catalytic wet air oxidation using carbon bead – supported iron nanoparticle – containing carbon nano fibers in an especially configured reactor. *Biochemical Pharmacology*. 4(2):1504–1513. doi.org/10.1016/j.jece.2016.02.021.

Yang, S, Wang, X, Yang, H, Sun, Y & Liu, Y. 2012. Influence of the different oxidation treatment on the performance of multi-walled carbon nanotubes in the catalytic wet air oxidation of phenol. *Journal of Hazardous Materials*. 233–234:18–24. doi.org/10.1016/j.jhazmat.2012.06.033.

Yang, S, Cui, Y, Sun, Y & Yang, H. 2014. Graphene oxide as an effective catalyst for wet air oxidation of phenol. *Journal of Hazardous Materials*. 280:55–62. doi.org/10.1016/j.jhazmat.2014.07.051.

Ye, J, Mu, Y, Cheng, X & Sun, D. 2011. Treatment of fresh leachate with high-strength organics and calcium from municipal solid waste incineration plant using UASB reactor. *Bioresource Technology*. 102(9):5498–5503. doi.org/https://doi.org/10.1016/j.biortech.2011.01.001.

Yu, Y, Wei, H, Yu, L, Gu, B, Li, X, Rong, X, Zhao, Y, Chen, L, et al. 2016. Catalytic wet air oxidation of m-cresol over a surface-modified sewage sludge-derived carbonaceous catalyst. *Catal. Sci. Technol.* 6(4):1085–1093. doi.org/10.1039/C5CY00900F.

Zapico, RR, Marín, P, Díez, F V & Ordóñez, S. 2015. Influence of operation conditions on the copper-catalysed homogeneous wet oxidation of phenol : Development of a kinetic model. *Chemical Engineering Journal*. 270:122–132.

Zarca, G, Ortiz, I & Urtiaga, A. 2015. Behaviour of 1-hexyl-3-methylimidazolium chloride-supported ionic liquid membranes in the permeation of CO_2, H_2, CO and N_2 single and mixed gases. *Desalination and Water Treatment*. 56(13):3640–3646. doi.org/10.1080/19443994.2014.978820.

Zhang, M, Dong, H & Geng, Z. 2019. Computational study of particle packing process and fluid

flow inside Polydisperse cylindrical particles fixed beds. *Powder Technology*. 354:19–29. doi.org/https://doi.org/10.1016/j.powtec.2019.05.061.

Zhou, H, Wang, G, Wu, M, Xu, W, Zhang, X & Liu, L. 2018. Phenol removal performance and microbial community shift during pH shock in a moving bed biofilm reactor (MBBR). *Journal of Hazardous Materials*. 351(October 2017):71–79. doi.org/10.1016/j.jhazmat.2018.02.055.

Zuo, K, Chang, J, Liu, F, Zhang, X, Liang, P & Huang, X. 2017. Enhanced organics removal and partial desalination of high strength industrial wastewater with a multi-stage microbial desalination cell. *Desalination*. 423(May):104–110. doi.org/10.1016/j.desal.2017.09.018.

Appendix A: Experimental Parameters

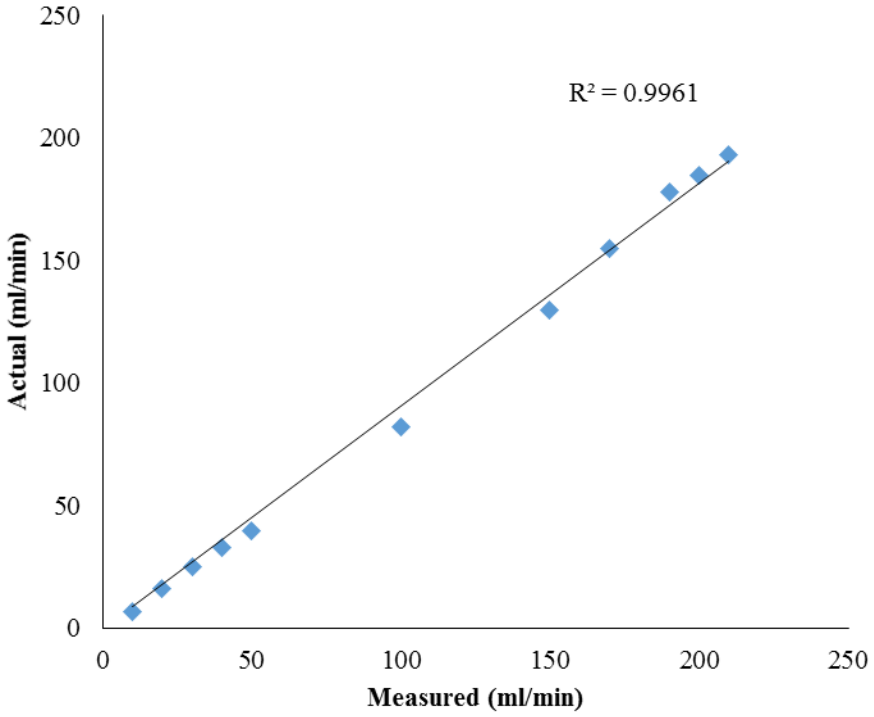

Figure 25: Pump calibration curve

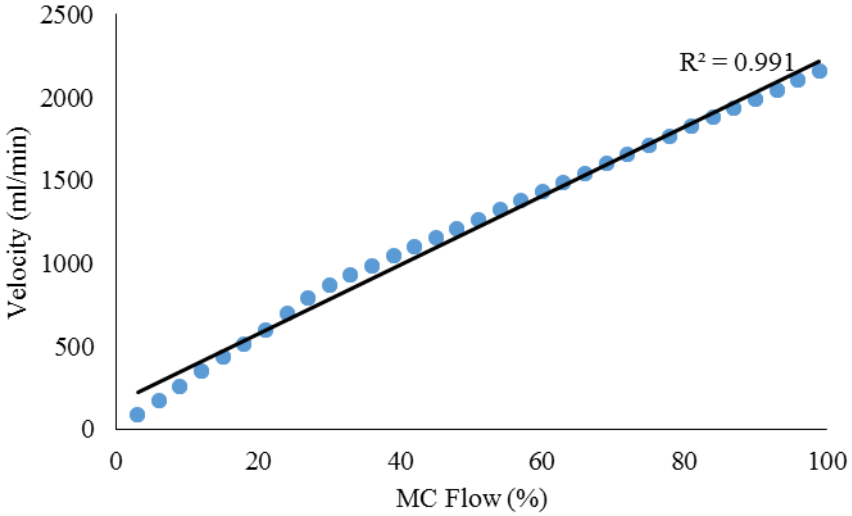

Figure 26: Mass flow controller

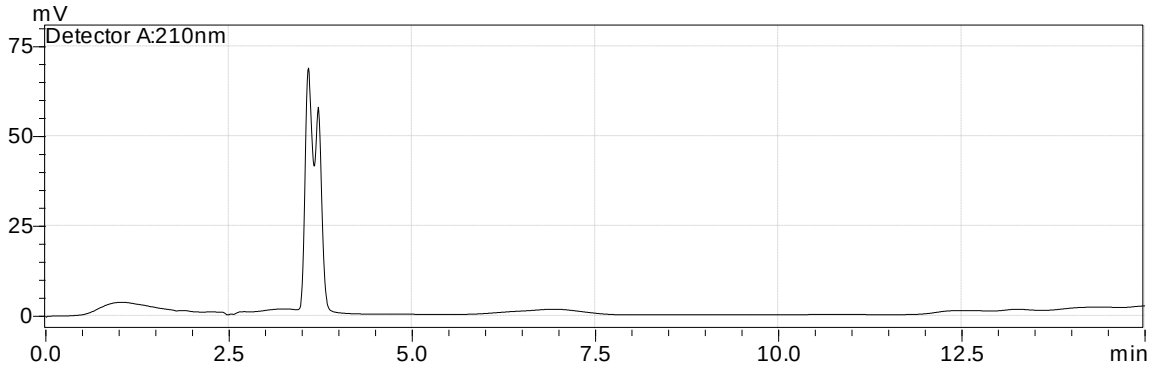

Figure 27: HPLC phenol retention time.

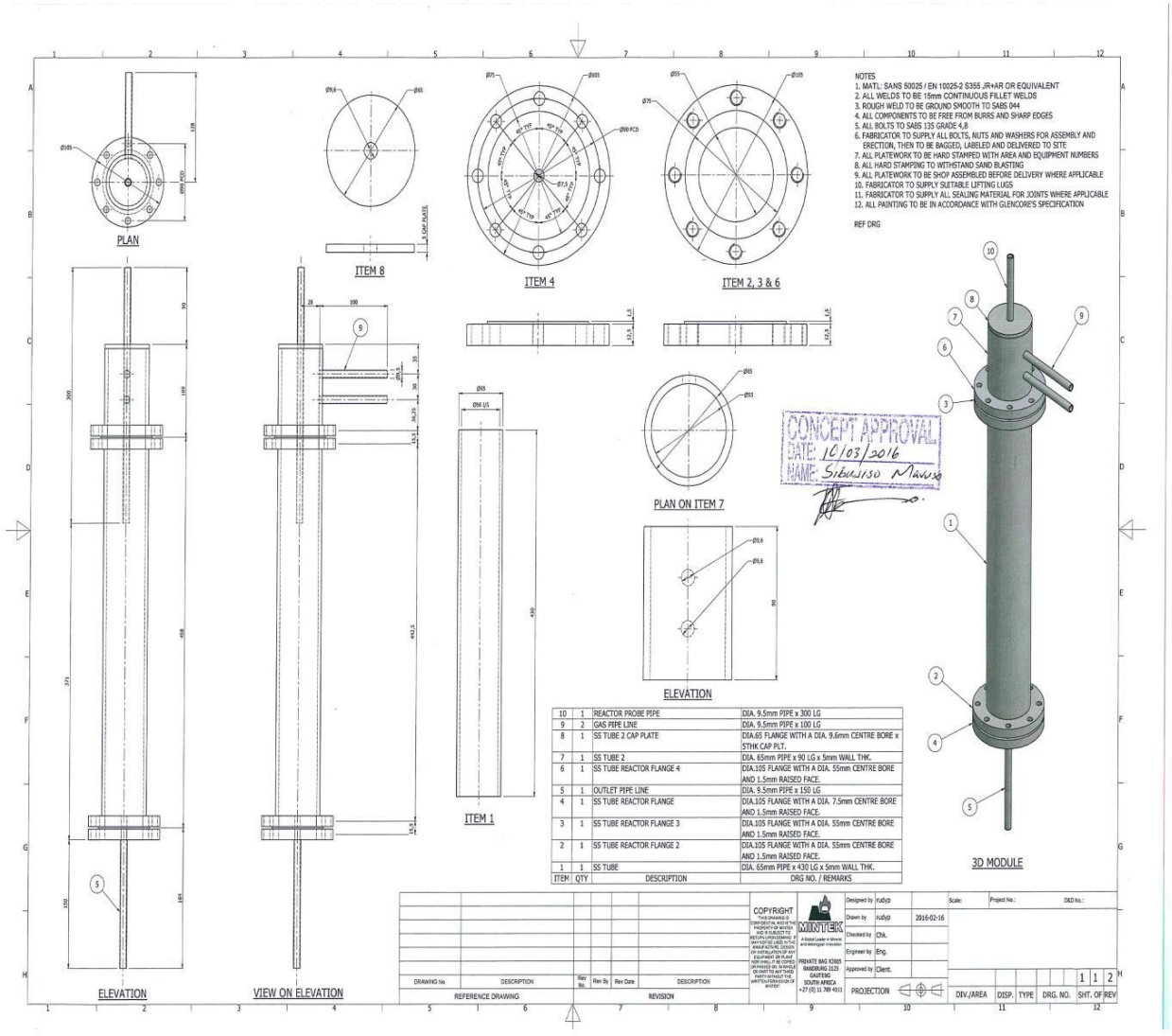

Figure 28: Reactor design.